INVESTIGATING THE EFFECTS OF TIO_2 ON THE STRUCTURE AND PROPERTIES OF SIO_2-P_2O_5-CAO-SRO-NA_2O BASED GLASSES

BY

KIEL DAVID SKELLY

A THESIS
SUBMITTED TO THE FACULTY OF

ALFRED UNIVERSITY

IN PARTIAL FULFILLMENT OF THE REQUIREMENTS
FOR THE DEGREE OF

MASTER OF SCIENCE

IN

BIOMATERIALS ENGINEERING

ALFRED, NEW YORK

SEPTEMBER, 2019

INVESTIGATING THE EFFECTS OF TIO_2 ON THE STRUCTURE AND PROPERTIES OF SIO_2-P_2O_5-CAO-SRO-NA_2O BASED GLASSES

BY

KIEL DAVID SKELLY

B.S. ALFRED UNIVERSITY (2016)

SIGNATURE OF AUTHOR_____

APPROVED BY_____

DR. ANTHONY WREN, ADVISOR

_____

DR. ALEXIS CLARE, ADVISORY COMMITTEE

_____

DR. STEVEN TIDROW, ADVISORY COMMITTEE

_____

DR. TIMOTHY KEENAN, CHAIR, ORAL THESIS DEFENSE

ACCEPTED BY_____

DR. GABRIELLE GAUSTAD, DEAN

KAZUO INAMORI SCHOOL OF ENGINEERING

ACKNOWLEDGMENTS

I'd like to thank the many people who've helped me through this thesis, both directly and indirectly. Firstly, my advisor Dr. Anthony Wren, he has allowed me to grow as a graduate student and the developed skills from working under him to solve problems. Others who have greatly aided me are my officemates, Sahar, Jeff, and Diana, I was fortunate enough to have you all to bounce ideas off of and make sense of my project. I'd also like to thank the technicians and professors who've taken breif moments to nudge me in a better direction, it has all added to my experience at Alfred. Others I'd like to thank are the plethora of friends I've made at Alfred over my time on campus, it truly was a great time and it was in large part due to the collective friendship we've made. My family deserves a nod as well, I can easily complain to them something technical but they're support and patience is more than I could have asked for.

TABLE OF CONTENTS

LIST OF TABLES

Page

LIST OF FIGURES

Page

ABSTRACT

Bioactive glasses have been researched and developed for dental and orthopedic applications since 1969. Current research has examined the substitution of non-traditional ions within the SiO_2-CaO-Na_2O-P_2O_5 which are suspected to improve the biological or material properties of bioactive glasses. This study examines four glass-ceramic compositions and the properties to understand the effects of increasing TiO_2 concentration when substituted at 20, 40, and 60 mol % into a Bioglass based composition.

Examining the structure of the glass shows that it is possible to achieve a fully amorphous material *via* melt quenching for concentrations up to 20 mol% TiO_2. The thermal working range of the glasses is expanded with 20 mol % TiO_2, 567 - 720°C, then the T_g window decreases as higher TiO_2 concentrations are incorporated into the glass, 605 - 705°C and 635 - 717°C for 40 and 60 mol % respectively. The mechanical strength is affected by the sintering temperature with 800 °C for the 20 mol % TiO_2 best matching trabecular bone strength with a modulus of 1.79(±0.16) GPa. Ionic release is negatively impacted by the addition of TiO_2, limiting the use of high TiO_2 compositions as a bioactive material. Comparison of the 0 mol % and 20 mol % samples show a slower release of ions and consequently deposition of ions in a manner that suggest bioactivity with incorporation of TiO_2 into the glass.

INTRODUCTION

1. What are Biomaterials?

"A biomaterial is a non-viable material used in a medical device, intended to interact with biological systems" is the definition laid out by Williams.[1] The material in each case will be dependent on the application, as hip replacements have different needs than a pacemaker. From this work the focus will be broadly on orthopedic replacement materials mainly bioactive glass and bioceramics. Orthopedic materials are used to replace bone and aid in the repair process, defining the purpose and giving context to what is needed for implant success. Current orthopedic replacements are either for full replacement of the bone, as a hip implant, or a fixture, like bone cements or surgical fixatives like pins, plates, or screws.[2]

The material selection for modern metallic implants include stainless steel,[3] CoCr alloy,[4] and Ti6Al4V.[5] These materials are selected because they have the mechanical strength to bear the load of bone, though too high of a strength may cause bone density loss and eventually implant failure.[6] One improvement in Ti-based implant is reduced elastic modulus to only 150% of natural bone.[7] This method of failure has been a driving force for research into other materials that will avoid stress shielding while still solving the other demands of an implant.

The lifespan of an implant is currently above 10 years, meaning surgical revision is another issue for device failure that future implants need to address as implants fail.[8] The focus on the integration of implants to aid bone tissue by leveraging chemical and biological factors so that the natural tissue can replace the implant, to eliminate the need for revision surgeries.

2. Bioinert / Bioactive / Bioresorbable.

Biomaterials fall into three distinct categories to qualitatively measure reactions: bioinert, bioactive, and bioresorbable. The least reactive is bioinert, having no reaction with the body, as the material does not degrade or affect the local tissue by not interacting

with the material, and the interaction *in vivo* is fibrous encapsulation of the implant to isolate the foreign material.[9] This level includes ZrO_2 based dental implants, as they are used for the color similarity to tooth but do not react with the biological tissue directly.[10] The next classification is bioactive, the material interacts with the local environment to promote cellular adhesion and integrating the biomaterial directly to the host tissue, like with bioactive glasses, leaching ions for osteogenic growth to occur on the surface.[11]

The third degree of interaction is bioresorbable, where the material is absorbed by the body over a period so that the material can be fully replaced with functional tissue. An example of a bioresorbable material is scaffolding for stent implants to prevent arterial collapse, that can be fully dissolved over 12 months.[12]

Bioactivity is a material property that indicates if a material is reactive within biological conditions. Bioactivity does not indicate whether the reaction is positive or negative, but rather does it occur. A better term is biocompatibility, this refers to a positive bioactive response in the desired situation. The bioactive properties allow the glass to degrade and re-deposit as a hydroxycarbonate apatite layer *in vivo* that interacts positively with osteoblast cells.[11]

Biocompatibility is another property that is worth mentioning as the prior paragraph only refers to the degree of interaction without including if the interaction is positive or negative. Biocompatibility defines the interaction as positive or negative including; adhesion, cytotoxicity, wear debris, or biochemical regulation toward certain pathways.

1. Bioactive Materials

Materials outside of metals such as glass and ceramic are researched for bioactive properties.

a. Bioactive Glass

Bioactive glass is designed to decompose in a way that aids osteogenesis, bone growth, through ionic leaching and formation of films rich with osteogenic ions that encourage osteoblast adhesion and bone remodeling. The origin of bioactive glass came from Larry Hench in 1969 as 45% SiO_2 24.5% Na_2O 24.5% CaO 6% P_2O_5 as wt %.[11] The success of the composition is the dissolution of CaO and P_2O_5 from the glass that redeposits as a hydroxyapatite-like layer on the surface.[11] This basis, referred to as 45S5, has been

tailored by compositional changes and ionic substitutions for property modification, such as mechanical strength, biocompatibility, and anti-bacterial properties.[13-15]

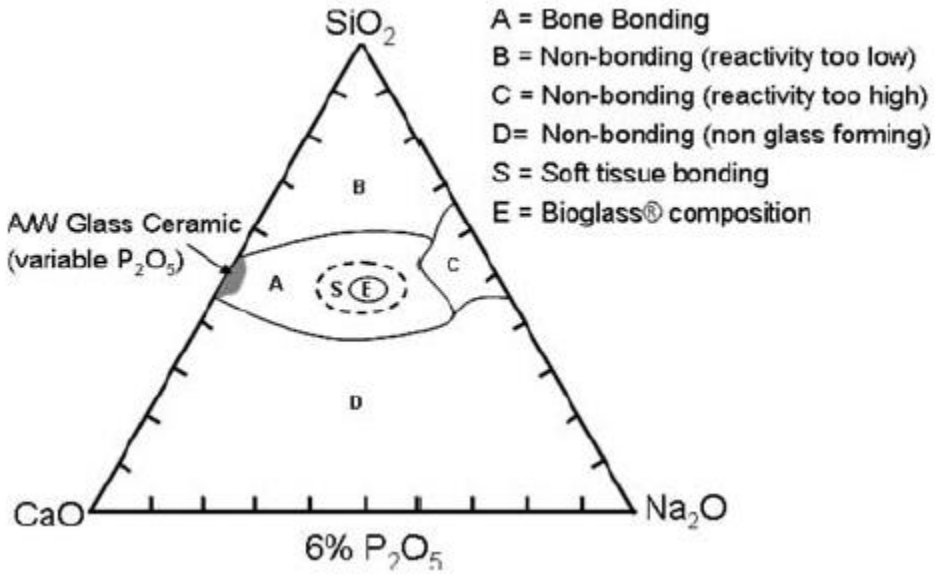

Figure 1. Ternary diagram of SiO_2-CaO-Na_2O at 6% P_2O_5 [11]

Bioactive glass chemically interfaces with the bone tissue and cells to begin the degradation process, the glass initially leaches ions and leaves behind a silica and hydroxycarbonate apatite layer, which encourages cell adhesion and remodeling.[11] From this the downstream effects, like the immunological response time, to regulate and encourage osteogenesis at the implant site.[11]

Bioglass and its derivatives rely on releasing ions for bioactivity and the observed biocompatibility. Aside from osteogenesis, bioactive glasses also promote angiogenesis and acts as an antibacterial agent. The precise routes of each function are dependent on which ion or compound is released, Ca^{2+} and PO_4^- are osteogenic because they form hydroxyapatite. Additionally bioglass having high silica content also improves osteoblast differentiation and adhesion.[16]

b. Bioceramics

Metals have issues with corrosion due to chemical and physiological conditions.[17] Ceramics are often used in lieu of metals because of the increased wear resistance and

chemical resistance, in biomedical applications this is seen as dental crowns.[18] For arthroplasty applications use of Ytrria-Stabilized Zirconia, YSZ, has been in use since the 1980's because of its ability to limit crack growth by forcing morphological changes at the atomic level extending the lifespan and limiting failures of the implanted device.[19]

Calcium phosphate, CaP, materials are also seen as a viable implant due to the chemical similarity of inorganic phases to bone. These CaP phases are often categorized based on the ratio of Ca:P, ranging from 0.5 to 2.0 and bone comes in at 1.67 Ca:P ratio. The ratio is a quick gauge for degree of degradation as well, with 0.5 being a quick dissolution and 2.0 being bioinert.[20]

c. Bioglasses v bioceramics

Bioceramics are more difficult to break down *in vivo* and with the trend toward bioresorbable materials glasses offer greater interaction with the biological medium. Ceramics based on calcium phosphates, $CaPO_4$, are bioactive though the degradation is very limited and only a surface phenomenon, with most coatings at 100μm thickness to achieve bioactivity.[20] Bioglass shows enhanced resorption rate with $CaPO_4$ cement composites than $CaPO_4$ cement alone.[21]

Bioactive glasses release ions rapidly, which forces a pH increase locally *in vivo*, this increase helps to further the breakdown of the silica network contributing to the bioresorbable properties.[22] Where ceramics are slow to release ions and is facilitated by cellular interaction

3. Bone structure, composition, and properties

Bone is composed of organic and inorganic components, collagen is the primary organic phase and hydroxyapatite comprises the inorganic phase. Hydroxypatite (HA), $Ca_{10}(PO_4)_6(OH)_2$, is the ceramic phase that gives the compressive strength for compressive loading. The structure of bone is dependent on which bone and what typical forces are expected, however the simplest distinction of bone can be either a dense, cortical. or porous, trabecular, bone. This leads most research to examine bone isolated as cortical or trabecular samples. Collagen type I bundles, composed of five triple helices approximately

100 μm length and 100 nm in diameter, serve to bind HA nano-crystals together to create the microstructure.[23]

Figure 2, shows that the structure and organization that is done by bone as it forms, this compounds the difficulty when designing for othropedic materials as these features will likely be in intimate contact with a device.

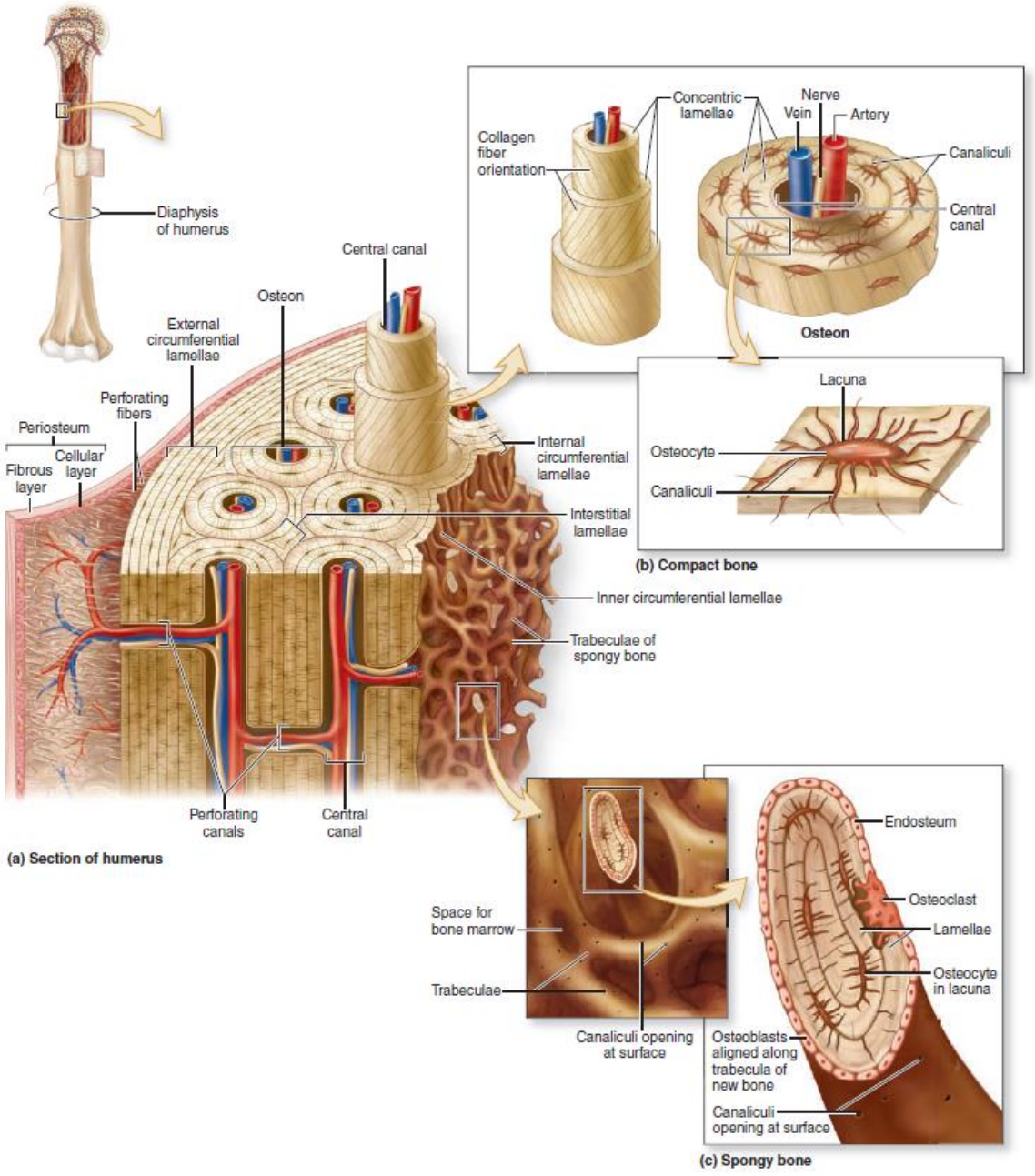

Figure 2. Structure of natural bone [24]

1. Hydroxyapatite

HA naturally occurs in bone as the primary inorganic phase, and consequently the mechanical properties of bone are dependent on hydroxyapatite, this makes it an obvious choice for bone replacement. However, the limited interaction with HA implants and bone prohibit using it as a bioresorbable material. The Young's modulus of HA varies from 35 to 120 GPa, well above cortical bone, 18-22 GPa.[20] The fracture strength of HA (1.2 MPa $m^{1/2}$) is lower than bone (2-12 MPa $m^{1/2}$) as well, likely due to collagen content in bone being less brittle than pure HA.[20]

Osteoconduction, bone growth, has been observed on porous HA samples with micropores, the reasoning being that the increased proximity to the "nearest neighbor" would allow the local concentration of Ca and P ions to accumulate and precipitate as apatite-like layer onto the scaffold. Mechanically, the evolution of the scaffold as degradation occurs has obviously decreased from the as manufactured samples.[25] Nanoindentation on bone for elastic modulus, from cadaver femurs aged between 53-93 years old, and determined that the average hardness of bone ranges from 0.4 to 0.829 GPa.[26] HA ranges from 42.2 – 81.4 GPa across sintered samples between 1150 – 1300°C.[27]

a. Mechanical properties

Because of the loading that bone undergoes the mechanical properties are the primary focus for creating a successful orthopedic device. The elastic modulus has been most studied for bone, is accepted as ranging between 35 and 120 GPa.[20] The biaxial flexural strength (BFS) for bone is less studied, however because BFS examines the strength over a larger area where 3 point bending only loads along one axis, comparisons can be made between the two tests.[28] Cortical bone drives the mechanical properties of bone setting it as the target for orthopedic implants. The ultimate stress in tension and compression are rather different for whole bone, 92.25 MPa and 153 MPa respectively, and strength decreased with increasing porosity.[29] Another study directly compared tensile (111.3 MPa), compressive (149.1 MPa) and flexural (223.4 MPa) tests.[30] With additional studies comparing cortical (130-180 MPa compression, and 50-151 MPa tension) and trabecular (4-12 MPa compression, 1-5 MPa tension) a more generalized model for bone can be established.[31]

The response of bone to mechanical stimuli is as a quasi-brittle material.[32-34] Meaning bone can withstand low strain, approximately 0.3%, and will fracture at higher strains, >2%.[35] Compressive loads are most common, though can be subjected to torsion or tension to failure. Bone is also anisotropic, because the lamellae layers alternate between parallel to bone and orientated off the parallel axis of the Haversian canal.[36] A common load for bone is approximately 4 MPa, though can increase dependent on activity, with forces peaking at 3 times body weight.[37]

Bone reacts to loading to strengthen or weaken, Frost et al. proposed that remodeling is linked to micro-strain. The ideal strains from Frost claim that between 2000-3999 με produces cortical bone.[38] Additionally, a study done on rat ulnae showed cyclic loading was optimal to encourage bone growth compared to static loading conditions.[39]

The mechanical demands of bone vary by composition; trabecular bone elastic modulus that ranges from 1- 2 GPa, and compressive strength ranging from 1 – 100 MPa.[40] Where cortical bone ranges 100 – 230 MPa compressive strength and 7 – 30 GPa elastic modulus.[41]

b. Stress Shielding

Also known as Wolff's Law, stress shielding is a phenomenon that occurs when there is a mis-match of elastic modulus between an implant and natural bone. This mis match causes the bone that is not undergoing loading and gradually lose bone mass through remodeling. The exact biological process is not well understood, but it is thought to be influenced by fluid pressures in local bone, either hydrostatic or interstitial fluid flow.[42] From this under-loading of bone a decrease in mechanical strength over time is observed, this is a concern with larger and permanent implants. Wolff suggested bone is self-optimizing, and this is now understood as bone metabolism or remodeling.

2. Bone remodeling

Because bone is such a complex system key terms have been developed to explain the stages of bone remodeling. The simplest bone-implant relation is *osteointegration*, defined by having the bone firmly anchored to the implant, this fixes the implant to the surrounding tissue. The next goal is to promote *osteoconduction*, migration of osteo-type cells into the implanted volume, which will give a stronger anchor for the integration and

decrease risk of aseptic loosening. *Osteogenesis* refers to differentiation into osteo-type cells from the nearest cellular lineage and subsequent bone deposition and remodeling phases, *osteointegration* is the furthest goal for bone remodeling as this treats the implant as native tissue.[43]

Bone remodeling process is a multi-stage process, as detailed in Figure 3, beginning with the secretion of cytokines that activate osteoclast precursors to begin forming into osteoclasts and migrate to bony surfaces (activation).[44] Once attached to the bony surface osteoclasts release hydrogen and phosphatases that cause an acidic pH to aid enzymatic decomposition of the bone tissue leaving a pitted surface (resorption).[45] After the resorption stage the pitting exposes mononuclear cells that differentiate to macrophages which do finer cleaning than osteoclasts can (reversal), at this point the bone has been cleaned and osteoblasts begin depositing a new bone layer (formation). The final stage (termination) is reached when the resorption and deposition rates equilibrate.[44] It is speculated mechanical loading influences remodeling which is seen in stress shielding, where rigid implants weaken the anchoring bone through elastic modulus mis-match.[46]

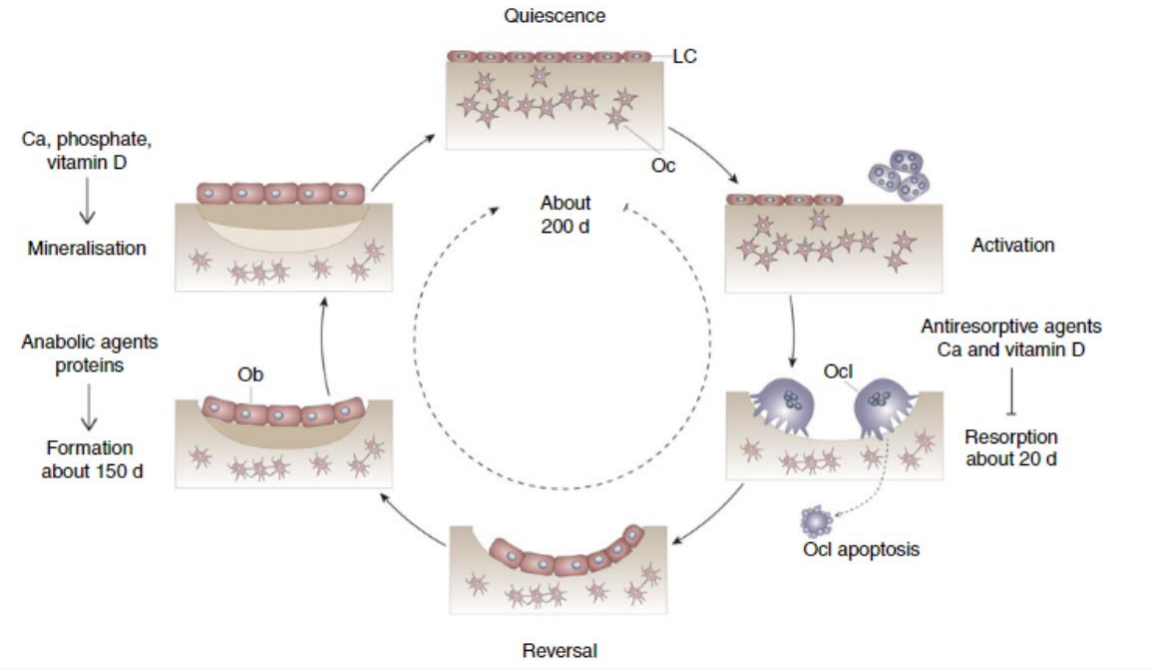

Figure 3. Bone remodeling process of natural bone [47]

Osteoclasts have also been shown to remove on average 29 μm of bone depth and a surface area of 10,876 μm^2 when exposed to the hormone RANKL,[48] this pitting can provide mechanical anchoring points for osteogenic ingrowth to cement the implant firmly.

4. Ions For Therapeutic Effects

Therapeutic effects can be achieved through ionic release of bulk bioactive glass surface reacting with *in vivo* cells and fluid. The effect is strongly related to the ion released, concentration, and ability to remove the ions to prevent cytotoxic accumulation. Generally, the aforementioned ions in 45S5 are all considered to be beneficial to bone growth and serve as a basis for other bioactive glass compositions.

Calcium and phosphorus are major components of bone, as $Ca_{10}(PO_4)_6(OH)_2$ or hydroxyapatite,[20] from a bioactive glass the released ions promote the deposition of CaP rich film that is converted into hydroxy carbonate apatite, which gives bioglass osseointegration properties.[11] Making these ions ideal for the inclusion in bioactive glass compositions.

Strontium is used as osteoporotic medication in the form Strontium renalate, which downregulates osteoclast activity by 30% in isolated rat cells and has increased differentiation to pre-osteoblast cells, MC3T3-E1. In humans the alveolar bone showed a decreased resorption rate and increased surface area for mineralization, which also increased bone mass and mechanical strength.[49] From this clinical and laboratory evidence there is solid rationale to include Sr^{2+} into a bioactive glass. Strontium as a dopant in 45S5 has also shown lamellar bone growth compared to woven bone growth on un-doped 45S5.[50] Additionally strontium is similar in size and charge to calcium, 0.118 nm to 0.100 nm respectively and both having +2 charge.[51]

Silicon has been shown to promote collagen synthesis and used as a gel promotes osteoblast differentiation. The biochemical regulation of silicon also positively correlates with bone mass density with osteoporotic patients when introduced from dietary changes.[52] The use of silicon has origins in bio-glass from Larry Hench with the composition of 45S5, bioglass.[53] Additionally, Si has been linked to skeletal development benefits as well when dietary intake was controlled in infant rats over 26 days and examined post-humorously.[54] Silicon is known to promote angiogenesis, vasculature growth, which is extremely helpful

in bone remodeling as vessels aid in removal of wastes and can bring in other materials to maximize the regenerative process.[55]

Sodium in the bone metabolic process has been linked to osteoblast differentiation. Decreasing the sodium concentration showed an upregulation of osteoblast activation, and thus bone growth.[56] Sodium is also being examined as an early detection sign of osteoarthritis through MRI measurements.[57] Sodium, is also tightly regulated *in vivo*, a normal Sodium level would range from 135 – 145 mmol/L, and decreased Na levels can promote osteoclast differentiation and activity.[56] Sodium also readily dissolves in aqueous solutions and the weak bond to oxygen helps expose a larger surface area to continue reacting and releasing other ions into solution and increase the overall interactions with the bioglass.

1. Titanium *in vivo*

The use of titanium (Ti) in orthopedics is not without limits: low shear strength, leaching from dopants, and wear rate can cause adverse effects on the implanted tissue, these issues limit the effective life of Ti implants to a decade.[7] The passivation of the surface however, can limit further leaching into the metallic bulk of titanium, which limits leaching of metallic ions into the surrounding tissue.

Titanium is not an ion (Ti^{4+}) that is naturally found *in vivo*, clinically titanium metals will naturally create a thin oxidized layer, or passivation layer, that will prevent ionic leaching from the bulk material. The passivated layer is also more stable, biologically speaking, allowing cell adhesion to TiO_2 opposed to fibrous encapsulation.[58] The risk of using an ion that is not native to a biological system is increased as there are many different interactions that can occur, however titanium is a more biologically acceptable material and does not invoke an immune response allowing osteointegration due to the promotion of ALP, osteopontin, and osteonectin that encourages osteoblast differentiation.[58]

Titanium shows excellent characteristics within a biological environment at the clinical level as implanted devices for dental implants or in TJA (total joint arthroplasty) for load bearing applications.[59,60] TiO_2 can precipitate apatite from SBF after treatment with H_2O_2 in low concentrations, 3-6 mass%, along with anatase phase.[61] One rationale to include TiO_2 has been from Boyan et al. where crystallized TiO_2 versus amorphous TiO_2

showed preference for chondrocyte adhesion and proliferation.[62] Typical studies of TiO_2 in glasses has been limited to low concentrations, < 5 mol %,[63-65] to remain glassy with some success. Going above these percentages, to 10 – 30 mass%, have often yielded partially crystallized glasses.[66-68] Previous studies have also shown that the addition of TiO_2 into a SiO_2-PO_4^{3-}-CaO-Na_2O glass ceramic shows increased antibacterial properties against *S. epidermidis* by inhibition zone measurements.[68] TiO_2 also shows increased bone bonding strength over commercially pure Ti-metal when used in orthopedic studies over 12 months.[69] Some research concludes that the slowed ionic release from Ti-doped bioactive glasses promotes osteoblast adhesion and proliferation.[70]

The addition of TiO_2 to the Bioglass based glass composition proposed in this work will be characterized in order to describe any significant benefits or drawbacks associated with its use in close proximity to natural bone for use as a regenerative material. This will be achieved by examining the material properties, such as crystal structure, ionic dissolution, glass-bonding, thermal behavior, and mechanical strength. Additionally, imaging will also be employed to describe and understand the surface dissolution and any mineral deposition.

EXPERIMENTAL PROCEDURE

1. Glass formulation

Three TiO_2 containing glasses (KS-20, KS-40, KS-60) and one control glass (KS-0) were formulated to understand the effect of TiO_2 addition on glass properties, compositions are listed in Table I. The dry reagents were weighed and mixed via rolling for at least 1 hour, then melted in a Pt crucible at 1500°C in Lindberg Blue M furnace for 1 hour then shock quenched in water. The frit was then dried and pulverized to pass a 45 μm sieve opening.

Table I. Mol % of Glass Compostions proposed in this study

mol %	KS-0	KS-20	KS-40	KS-60
SiO_2	45	35	25	15
TiO_2	0	20	40	60
P_2O_5	1	1	1	1
CaO	23	19.67	16.33	13
SrO	10	6.67	3.33	0
Na_2O	21	17.67	14.33	11

2. Glass charaterization

1. X-ray diffraction

X-ray diffraction was done via a Bruker D2 from $10° < 2\theta < 70°$ at a step size of 0.02 with a 1 sec scan per step while rotating at 60 rpm with glass powders held in a stainless-steel sample holder. Voltage was set at 40 kV and amperage was set at 40mA, with a Cu Kα1 source ($\lambda = 1.54Å$) and LynxEye detector.

2. Disc preperation

To form disc samples, 0.4 grams of each powder were pressed into 12mm diameter molds at 10 tonnes and sintered for 24 hours at 600 °C, 800 °C and 1000 °C, with a

10°C/min step rate during the sintering profile. A Lindberg Blue M type furnace with 5 discs of each composition and multiple temperatures were used for sample treatment. Several discs of 6 mm diameter and 0.1g of powder pressed at 3 tonnes were also sintered at 600 °C for 24 hours were made to be submerged in varying pH solutions, detailed later.

3. Biflexural strength

The method laid out by Williams et al.[71] with a 1mm/min crosshead speed on an Instron 5566 P6016 10kN load cell with 5 discs to determine the biaxial flexural strength and modulus. Discs of 12 mm diameter were fractures and thickness was measured prior to testing at 3 points per disc (*n=5*) to determine thickness for calculations. The equation used is as follows:

$$BFS = \frac{F}{t^2} * (0.63 * ln\left(\frac{R}{t}\right) + 1.156) \quad (1)$$

Where F is force in Newtons, t is thickness in mm, and R is radius of supports. Additionally, biflexural modulus was calculated from Choi et al.[72] for ball on ball biaxial flexure from this equation:

$$E_{BF} = \frac{\beta P a^2}{\omega h^3} \quad (2)$$

Where β is the center deflection function of the disc, P is the maximum load failure, a is the ring support radius, ω is the center of disc deflection, and lastly h is disc thickness.

4. Particle size analysis

Beckman Coulter Multisizer 4 was used to obtain an average particle size, D10, D50, and D90 information for each powder with *n = 3*, the aperture opening measured 100 μm diameter. Each sample was suspended in an electrolytic solution (NaCl) at 25 °C and stirred during the measurement to ensure an even distribution of particles in suspension.

5. Magic Angle Spinning Nuclear Magnetic Resonance

Bruker Avance III 600 with an Ultrashield Plus solid-state NMR magnet and probe diameter of 4mm. The ^{29}Si channel had a frequency of 600.20 MHz, while the proton channel had a frequency of 119.29 MHz. Polydimethylsiloxane was used for reference. A low power decoupling was used for each sample, which spun at 7.0 kHz and had an

applied pulse length of 75°. For KS-0, KS-20 and KS-40 a relaxation time of 60 seconds was used for 300 scans. KS-60, due to high Ti content, had a relaxation time of 120 seconds for 300 scans.

6. Differential Scanning Calorimetry

SQT 600 instrument heated samples from ambient temperature at 10°C / min to 1050 °C in Pt pans in ambient atmosphere. The data was recorded was analyzed via TA universal software, to find the glass transition temperature, T_g, and crystallization temperature, T_c, of each composition.

7. Inducitvely Coupled Plasma

Perkin Elmer Optima 8000 on each glass after DI water immersion for 1, 10, 100, and sample flow rate of 1.5 mL/min were analyzed and spectral results were analyzed. Each powder was controlled such that 10mL of deionized water had $1m^2$ surface area per glass powder. Each ion examined and 1000 hours with n = 3 for each glass and timepoint. A plasma flow rate of 12 L/min (Ti, Ca, Na, Si, P, and Sr) was calibrated for 1, 10, 100, and 1000 ppm concentrations and de-ionized water as a control, 0 ppm.

8. Brunauer-Emmett-Teller theory

All glasses were subjected to N_2 adsorption for surface area analysis after N_2 purging for 1 hour in FlowPrep 060, each glass was massed prior to experimentation, samples were then loaded into a Micrometrics Tristar 3020.

9. Scanning Electron Microscopy & Energy Dispersive X-ray Spectroscopy

SEM/EDX was used to analyze the surface of samples post-aqueous corrosion testing. For this test, 6 mm diameter discs were prepared from KS-0 and KS-20 and sintered at 800 °C for 24 hours, the discs were then submerged in solutions of varying pH, 4,7,10 (HCl, deionized water, and NaOH respectively) as a test for precipitation on the different compositions at 1 hour, 10 hours, and 100 hours immersed in differing solutions. Desiccated for at least 24 hours at ambient temperature and then analyzed via FEI Quanta 200 SEM, Au-coated samples with 5kV images and 20kV EDAX analysis on selected features.

RESULTS AND DISCUSSION

1. Particle size analysis

The average particle size for each glass composition was found to be less than the 45 μm sieve used for particle processing as seen in Figure 4. Approximately 90% of the particles were under 30 μm, and the median ranging from 12 to 15 μm. One advantage that this may offer is a textured surface to promote cellular adhesion. The distribution in particle sizes could be beneficial for sintering and processing of the materials which will allow for the smaller particles to become embed within a solid matrix thereby promoting increased density, mechanical strength, and contact area for cell adhesion.

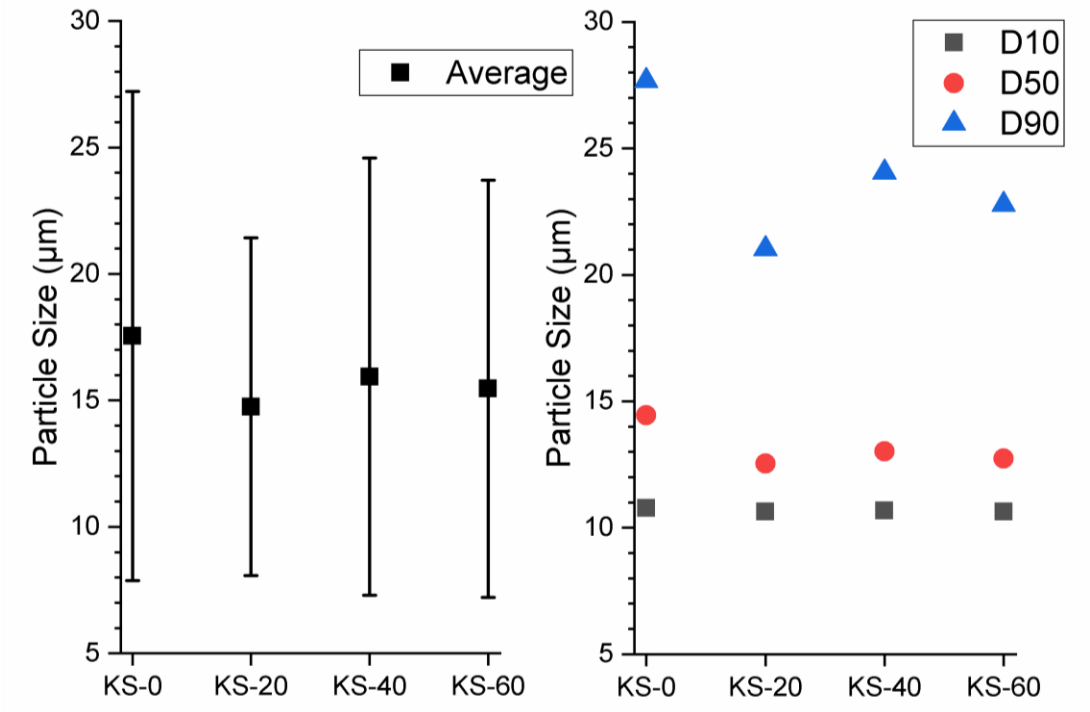

Figure 4. Particle size analysis with the average (left) and distribution (right)

2. X-ray diffraction

The diffraction patterns from x-ray diffraction are presented in Figure 5 and shows that this series of glass can produce an amorphous material from melt-quenching from 1500°C, as seen in KS-0 and KS-20. KS-40 and KS-60 presented $CaTiO_3$ phases in an amorphous matrix. At a sintering temperature of 600°C KS-0 still is amorphous and crystallinity appears in KS-20, KS-40, and KS-60 at 600°C with KS-20 no titanium is incorporated within the crystal structure. KS-20 shows that titanium forms crystalline structures at 800°C, and at 1000°C some strontium substitutes in for the calcium location within the crystal phase. Similar experiments show that TiO_2 substitution for SiO_2 can also create an amorphous material.[66] The presence of an amorphous hump is seen with all materials at even 600°C, suggesting that is still below the crystallization temperature of each composition of glass.

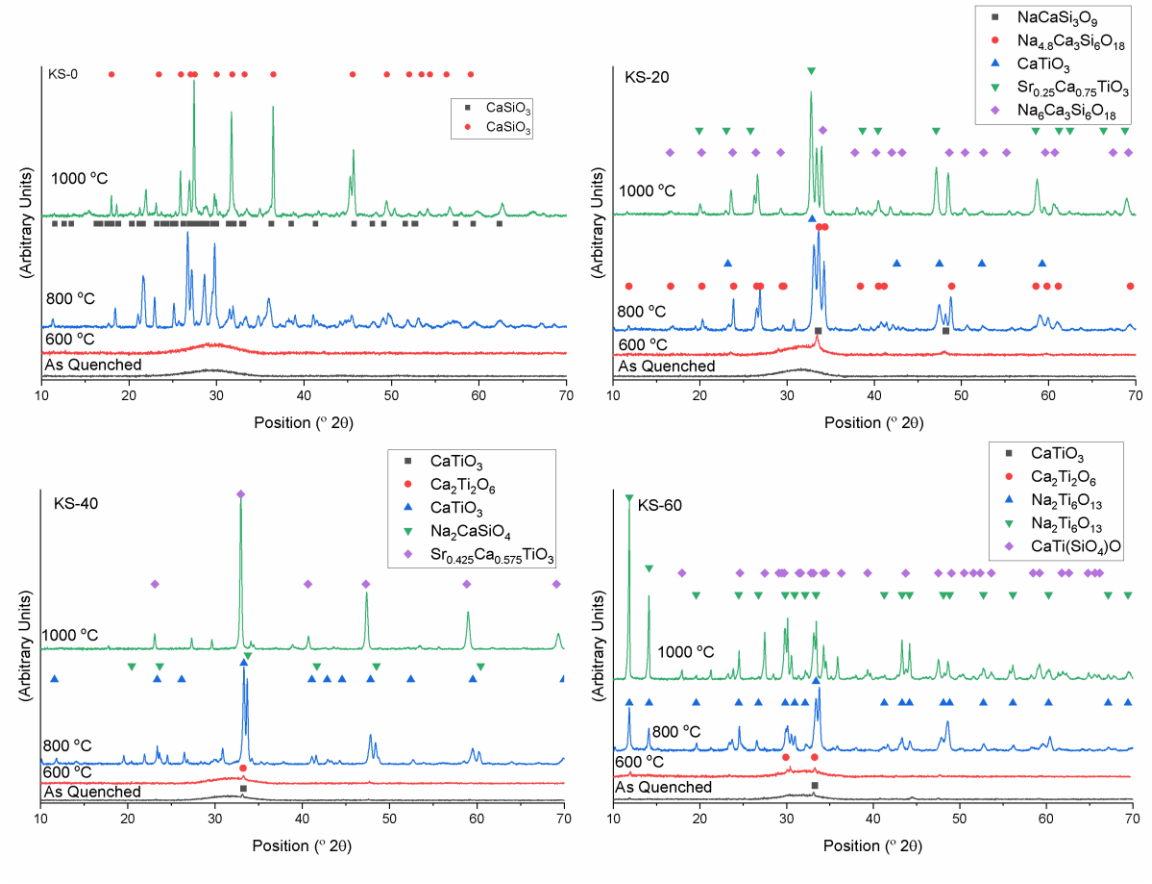

Figure 5. XRD of compositions with associated phases at labelled temperatures with the background signal removed

Distinct multiple phases appear in each composition and temperature, with a preference for Calcium and Oxygen appearing in most crystalline phases, usually with either Silicon or Titanium. $CaTiO_3$ appears in KS-20 beginning at 800 °C and 1000 °C, KS-40 from as quenched to 800 °C, and KS-60 as quenched and 600 °C meaning the largest challenge to keep a glassy phase is to prevent the formation of calcium silicates in KS-0 and KS-20, but there is little to be done with KS-40 and KS-60 regarding crystallization. Comparable crystal structures can be found with TiO_2-doped bioactive glasses with similar CaO concentrations that disappear when the CaO is replaced with Na_2O in the glass formulation.[73] Strontium did not seem to induce crystallization in KS-20 and KS-40 until 1000 °C suggesting that the incorporation of SrO may help to widen the glass transformation range of TiO_2-doped materials.

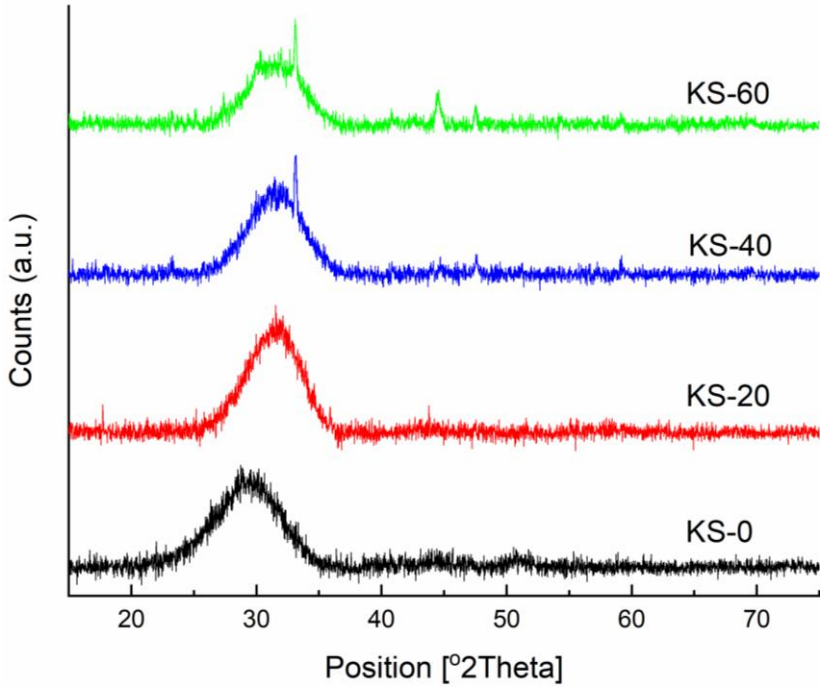

Figure 6. Comparison of KS-series as quenched

The as quenched and 600 °C samples show an amorphous hump in the XRD patterns with calcium titanite beginning to crystallize at 600 °C for all samples with any TiO_2 presence. The comparison of all quenched glasses, Figure 6, more clearly shows the $CaTiO_3$ peaks of KS-40 and KS-60, The shift from KS-0 to KS-20 indicates that TiO_2

narrows the amorphous hump, which may indicate the preference of TiO_2 to crystalize in this glass system.

3. Brunauer-Emmett-Teller theory

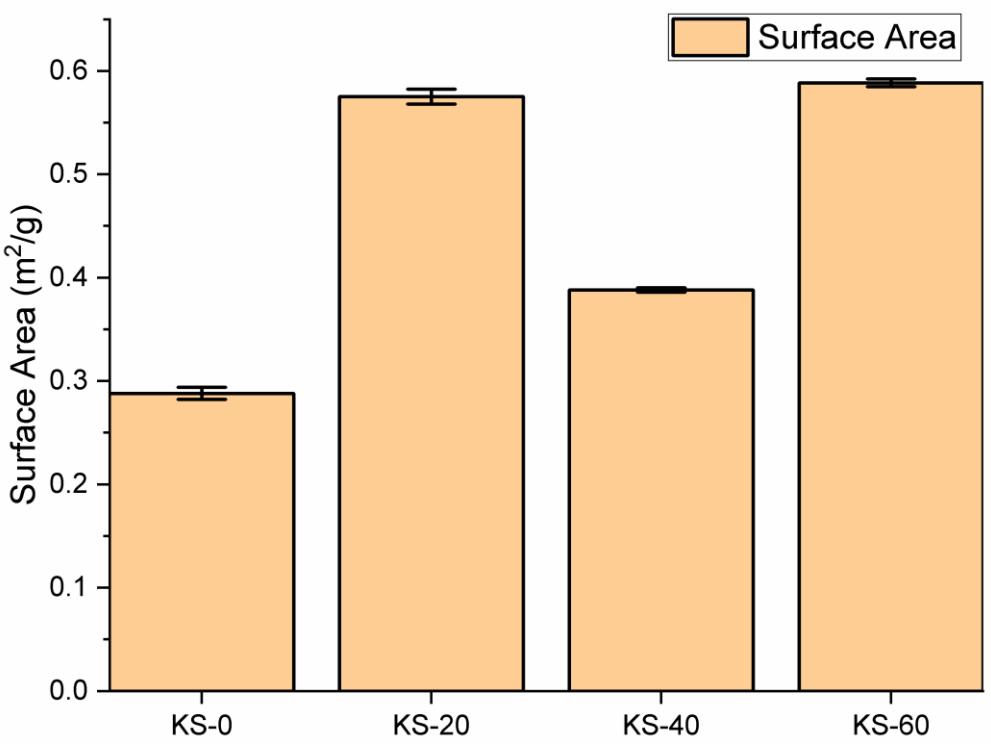

Figure 7. Surface Area Analysis done with BET method

Surface area analysis was conducted using Advanced Surface Area and Porosity measurements and the data is presented in Figure 7. This data presents the distribution in surface area of glasses as-sieved, that were later used for ICP-OES analysis and disc preparation. This data shows that slight differences exist between some of the processed samples. KS-20 and KS-60 have higher surface areas relative to KS-0 and KS-40. Though, these values are extremely low compared to mesoporous self assembled materials with surface area values of over 400 m^2/g,[74] and other similar SiO_2-CaO-P_2O_5 based solgel glasses with values around 100 m^2/g.[75] The possible advantage of having these glasses with a lower surface area may improve the sintering of particles for scaffolds and their use as an extrudable material for additive manufacturing processes.

4. Magic angle spinning nuclear magnetic resonance

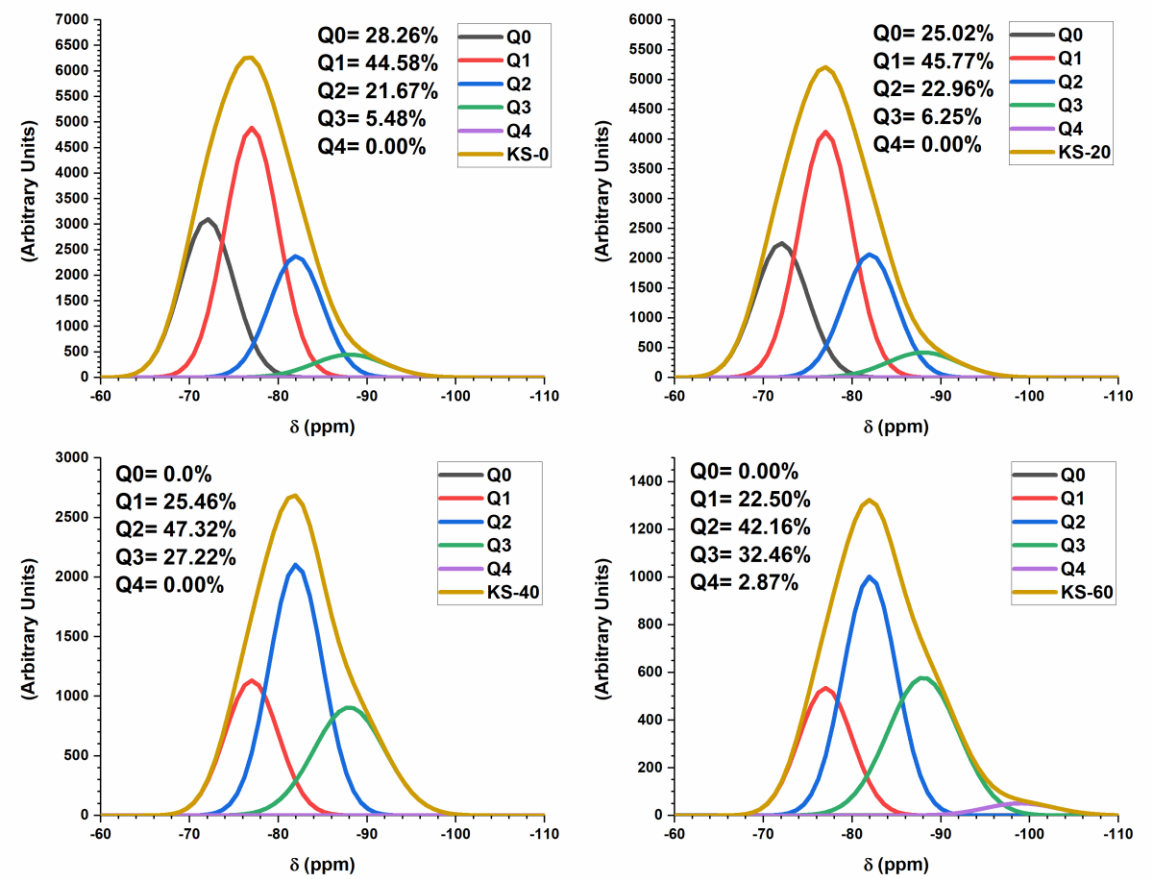

Figure 8. MAS-NMR data of each composition

The NMR spectra for each sample, Figure 8, show that with increasing TiO_2 content the Si^{4+} has increasing q-speciation, and the largest component of the bonding also increase from a Q^1 in KS-0 and KS-20 to Q^2 in KS-40 and KS-60, which compared to 45S5 is more bonded where Q^0 dominates the NMR spectra.[76] The 5 possible peaks for the combination for a full signal are a convolution of Q^0, Q^1, Q^2, Q^3, and Q^4 for ^{29}Si MAS-NMR found at -72, -77, -82, -88, and -92 ppm respectively. The only Q^4 species appears in KS-60 and is low relative to the present species of Si^{4+}, this suggests that Ti^{4+} is forcing Si^{4+} into crystalline structures. Also, since the Si^{4+} is the only ion being probed there is a decreased overall intensity directly related to the Si^{4+} content as seen in Figure 9. The shifting becomes more obvious when overlapping the deconvoluted images in Figure 9, where the

signal is shown to decrease substantially as SiO_2 is removed, the shift in speciation is unlikely to be affected by the lower signal making Ti^{4+} interactions with other ions more favorable than Si^{4+}. Shifting to lower ppm is also observed with increasing TiO_2 content,[66] indicating that there is a change in Si^{4+} bonding as TiO_2 is added, not solely a lower release due to Si^{4+} replacement. The favoring of low q-speciation for Si^{4+} has been linked to the formation of CaP layer and the depletion of cations from the silica network on the surface of bioactive glass.[77] The addition of TiO_2 to create a more bound silica network would make Ti^{4+} a network former, though the delayed increase observed in 40 mol% and above suggests that Ti^{4+} acts in an intermediate manner in the glass network.

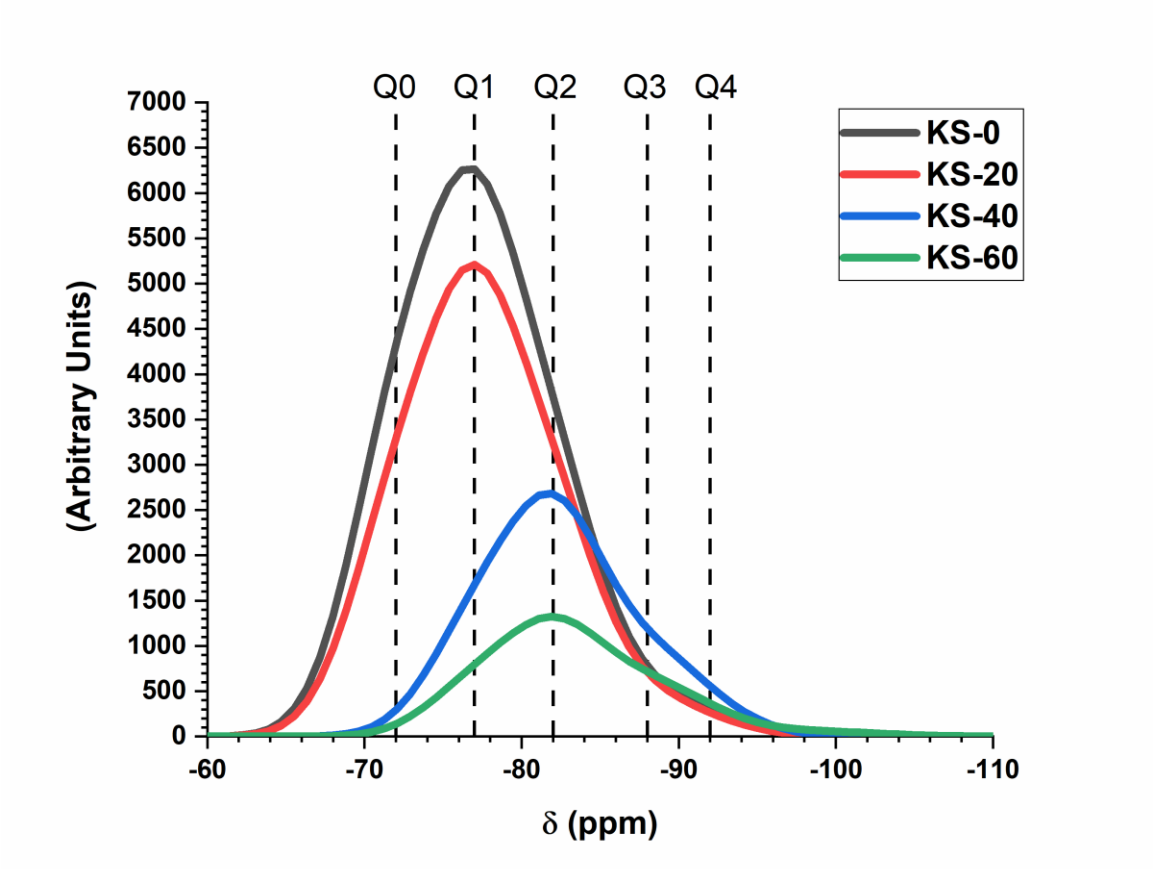

Figure 9. NMR spectra overlapped for all glass compositions

5. Differential Scanning Calorimetry

The thermal profile for each glass shows a processing window relative to the glass transition temperature and crystallization points for each composition, KS-0 from 685 – 775 °C, KS-20 has the widest range from 567 – 720 °C, KS-40 narrows to 605 – 705 °C, with KS-60 having the slimmest range from 635 – 717 °C. Beyond the crystallization temperature other phases that may be driving the shift in heat flow, but the primary interest is to keep a glassy material the first crystallization temperature is considered the most pertinent to this work.

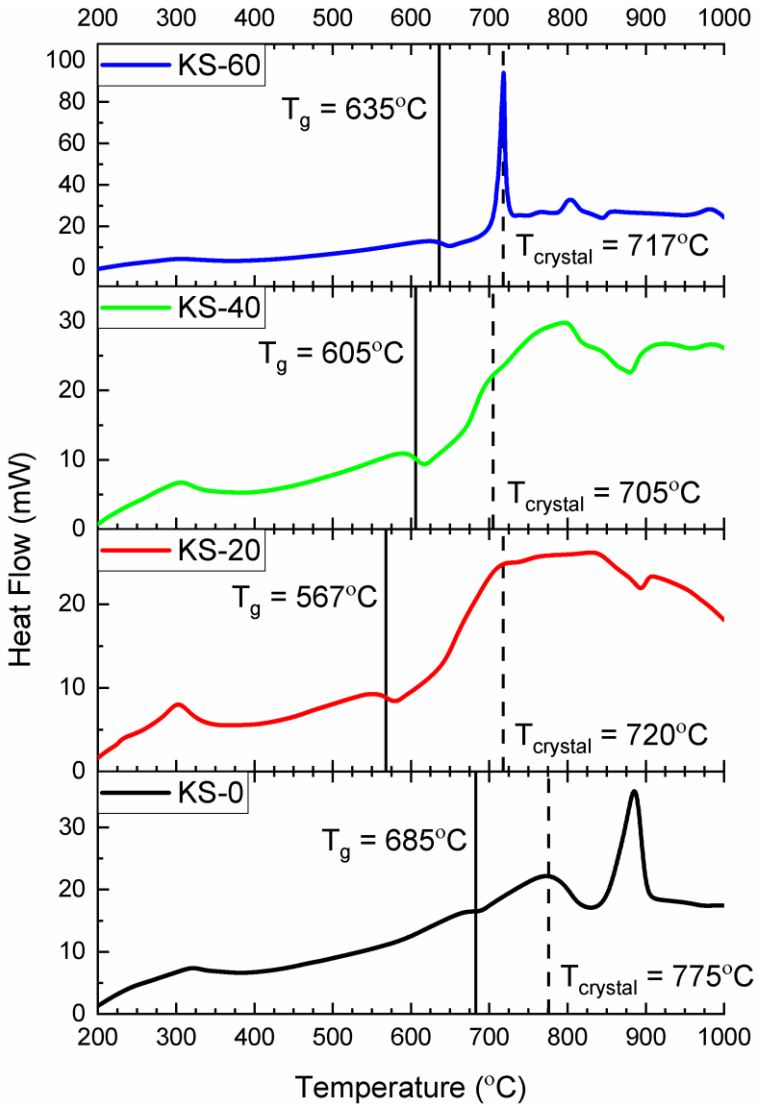

Figure 10. DSC for each composition

With similar glass ($33SiO_2$-$21CaO$-$32.5Na_2O$-$12P_2O_5$-$1.5MgO$) having a T_g at 634 °C and crystallizing at 830 °C,[78] the addition of TiO_2 here has shifted the range to lower processing temperatures available which can be beneficial when creating heat treated biomaterials such as scaffolds. Even compared to 45S5 the glass-ceramics here have a lower T_g and lower crystallization temperature.[79]

The addition of TiO_2 seems to initially drive down the T_g but then as the TiO_2 concentration increases so does T_g, indicating that concentrations of TiO_2 should be used near the 20 mol% level to achieve the widest window for T_g. This shift in T_g suggests that TiO_2 acts as a network modifier at a lower concentration, 20 mol %, and then acts as a network former for glasses as the concentration increases. The use of SrO in the mid-range compositions may be beneficial to expanding the T_g processing window as well, as one study reports a large increase when SrO replaces CaO for the glass working range.[80]

6. Biflexural strength

The biflexural strength of the material is shown in Figure 11, pertaining to equation 1, the forces shown reveal that the 600 °C sintering temperature resulted in extremely weak materials across all compositions, likely due to being below the T_g for all compositions as the discs are unlikely to be fully sintered and loosely bound together causing the low strengths observed, KS-20 as the exception to this due to being nearest the T_g (Figure 10). The highest strength materials occurred at 800 °C for KS-0, KS-20, and KS-40, whereas KS-60 peaked at 1000 °C. The biflexural strength of each composition drastically differs with sintering temperature, as previously stated in Figure 10, the 600 °C is below the T_g for all glass compositions. At the 1000 °C sintering an increase of mechanical strength is noted for the KS-60 only with the exact cause is assumed to be the majority TiO_2 concentration governs the mechanical properties.

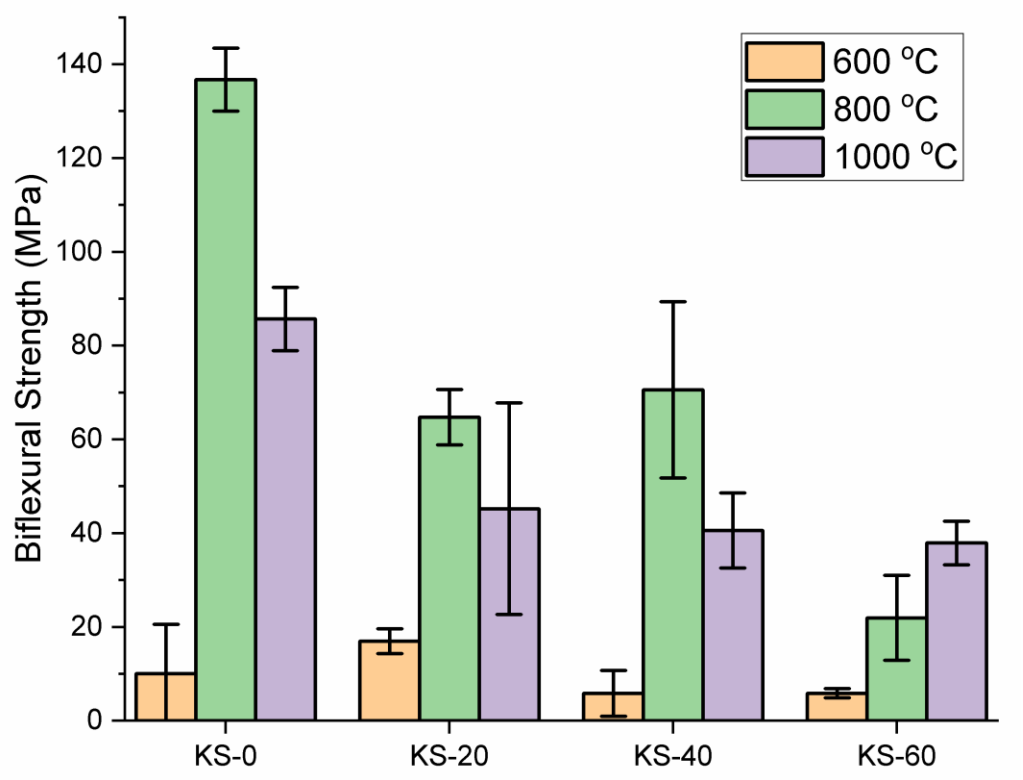

Figure 11. Biflexural strength of KS-series of discs after a 24-hour sintering profile

The modulus calculated from equation 2, Figure 12, have similar strengths however this distinction accounts for the material thickness and deflection from the disc center. KS-20 sintered at 800 °C shows similar modulus to trabecular bone (1-2 GPa), though all compositions fall short of the cortical modulus minimum of 7 GPa.[40] Compared to the flexural strength of hydroxyapatite KS-20 achieved a similar strength, 61.6 and 64.7 MPa respectively, at a lower sintering temperature of 800 °C versus 1250 °C.[81] The wide standard deviation in KS-40 800 °C is not recommended for load bearing applications, the source of the deviations is assumed to be processing defect related but is not examined here for the variation in disc strengths.

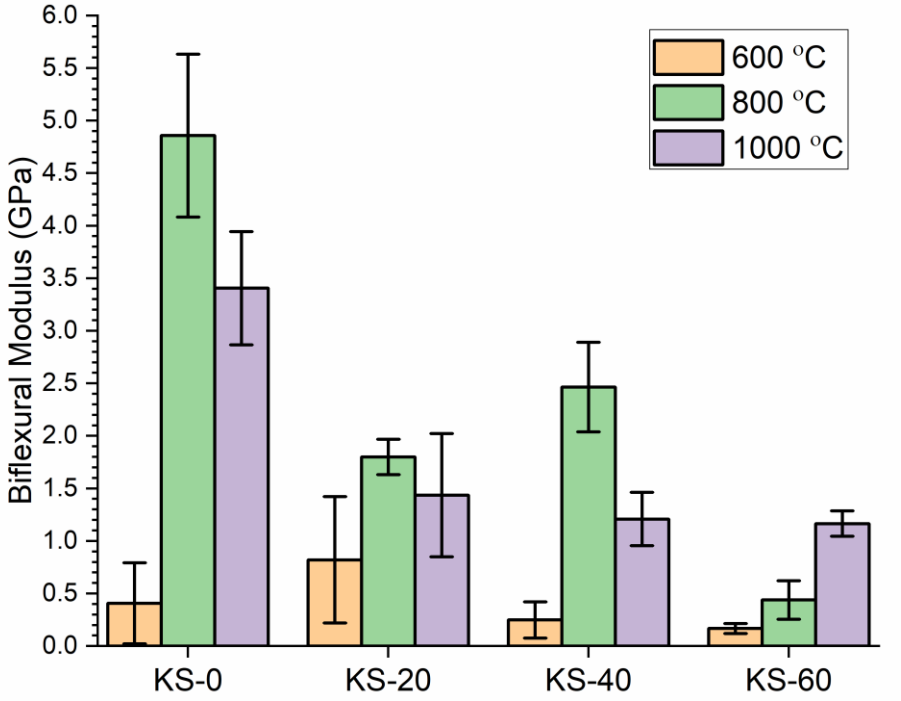

Figure 12. Biflexural modulus of KS-series of discs after a 24-hour sintering profile

7. Inducitvely coupled plasma

The release rate of all ions, Figure 13, shows that the release of silicon (Si^{4+}), sodium (Na^{+}), and phosphorous (P^{5+}) ions increase with time whereas strontium (Sr^{2+}), calcium (Ca^{2+}), and titanium (Ti^{4+})decrease with time. The release of Na^{+} reached the highest after 1000 hours from KS-0, indicating that Na^{+} is actively released by the glass and remains in suspension, likewise with Si^{4+} and P^{5+}, supported by other studies that also show similar trends.[66,82] Sr^{2+} and Ca^{2+} show peaks at 10 and 100 hours, respectively, this indicates that the ions have leached from the glass and then precipitated back out of solution, possibly forming crystals on the surface of the glass, since the samples were not agitated to prevent re-deposition. The general trend of all ions shows that the release of ions is negatively impacted by the addition of titanium in the glass. To further describe the effect of this approach would be to use SBF over DI water, as that is more biologically relevant. To contrast with another study by Li et al.[82] the ion release rates reduce and correlate more closely with crystalline behavior than amorphous releases.

The mechanism of glass particle dissolution is suspected by way of breaking oxygen bonds in Si-O-Ca or Si-O-Na primarily to initiate the dissolution of a glass,

however, addition of TiO_2 can slow this process and has been shown to be more insoluble in solution. Also, crystallization can limit the degradation rate, *i.e.* $CaTiO_3$ limits the Ca release as observed from TiO_2 containing glasses.[83]

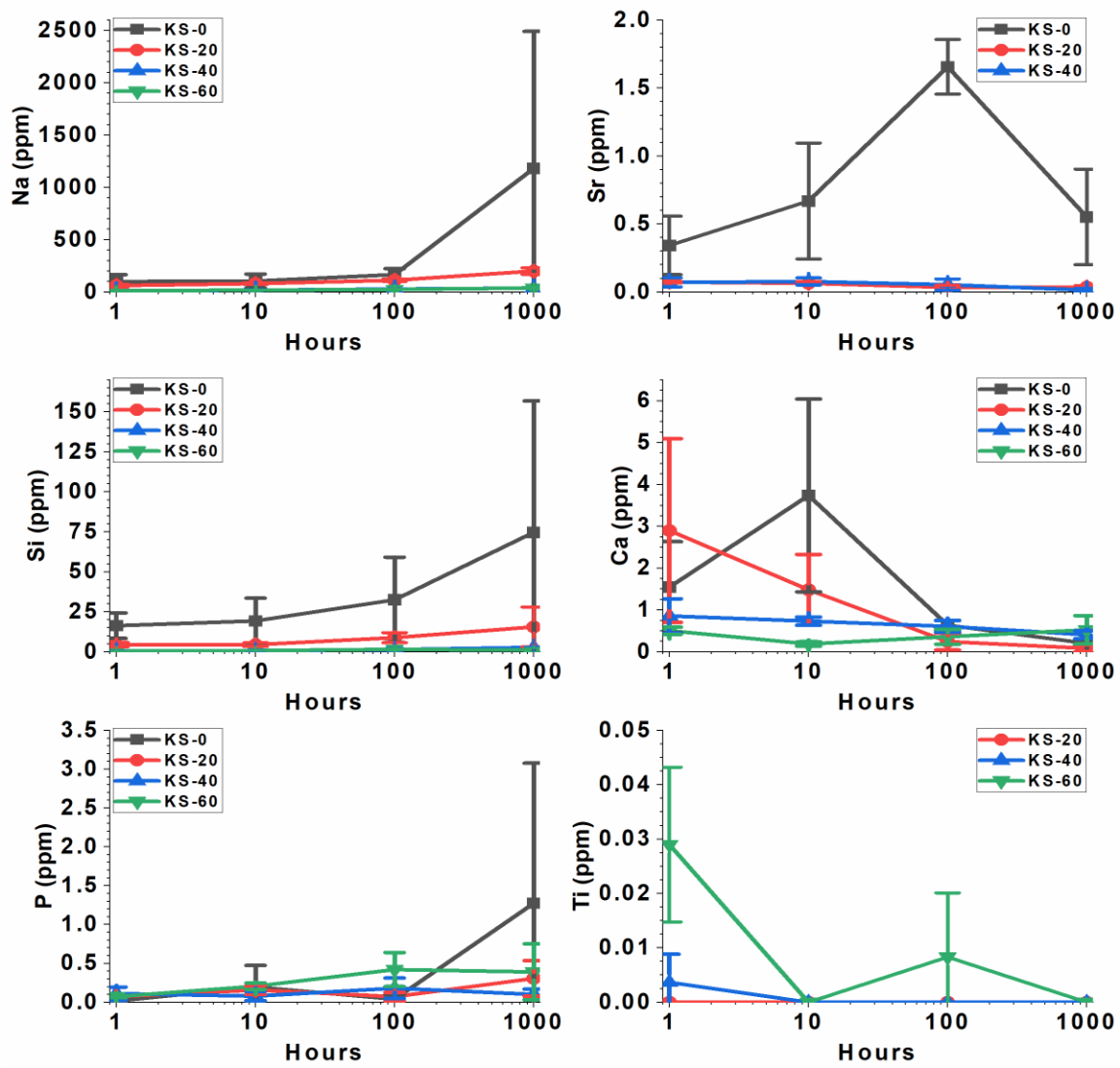

Figure 13. ICP data for each glass with $1m^2$ surface area over logarithmic time scale

The main reason to examine the release of ions is to provide evidence of approximate concentrations to the *in vitro* environment as the presence of ions in solution is known to favor certain cellular pathways.[84]

8. Scanning electron microscopy / Energy dispersive X-ray spectroscopy

The degradation of these glasses are important to understand at an ionic level, as done with ICP, and also at a microscopic level, with analysis from SEM and EDAX. The information gathered is about proving the glasses degrade in a manner that produces biologically relevant depositions that can be used with cells to aid in osteogenesis and other regenerative processes. Additionally, this examination shows if there is a preference for nucleation points or if the depositions is homogenous across the surface. Images can be found in the Appendix along with relevant EDAX spectra. EDAX signal similarity of Silicon (1.37 KeV) and Strontium (1.81 KeV) does complicate the distinction of which is present in the differentiation, which lead the focus on Calcium, Sodium, and Titanium for this experiment. Also, the low release ionic release rates from ICP for KS-40 and KS-60 excludes these compositions from analysis.

The KS-0 discs after 1-hour in all 3 solutions showed deposition of small sphere-like growths on the surfaces, Figure 14, 15, and 16. EDAX of the KS-0 discs at all pH's and times show that the deposits have significantly higher Calcium than the surface of the disc, however Calcium Phosphates had not formed due to the low Phosphate in the glass compositions (1 mol %).

Looking at the 10-hour samples for KS-0 the spheres, Figure 17,18, and 19, had grown larger and seems that the spheres could not support their own weight and collapsed onto the surface making bowl-shaped features on the disc surfaces. Some samples showed dendritic features that appeared at 10 and 100 hours and only when in pH 4 solution, Figure 17 and 20. The 100-hour KS-0 discs show an obviously crystalline deposit with less Sodium in the crystal and primarily Calcium. Lower Sodium concentrations are supported by the ionic release that shows continual increase over the 10-hour period.

KS-20 discs experienced a slower development of the same surface features, where KS-0 spherical features were apparent at 1-hour, the KS-20 samples lacked that stage and directly went to Calcium rich features that were like 100-hour KS-0 crystallized features with lower Silicon or Strontium relative content, Titanium also did not dissolve from the disc and redeposit over any period. At 100-hours the Calcium rich features can be seen

anchored to the discs, the nucleating point seems able to support multiple crystals, opposed to a large single crystal growth.

SUMMARY AND CONCLUSIONS

For this study four bioactive glass compositions were batched with varying TiO_2 concentrations (0, 20, 40, and 60 mol%) for melt quenching and characterized for use as a potential bioactive scaffolding material.

TiO_2 acts as a crystallizing agent in bioactive glasses, the main crystal that would develop at low annealing temperatures is $CaTiO_3$, but can still form a glass from melt-quench at 20 mol % TiO_2. From MAS-NMR data the KS-20 composition showed a similar glass connectivity to KS-0, suggesting TiO_2 in acts as a network intermediate in glass structures. Incorporation of TiO_2 does impact the properties of a glass and forces crystallization at lower temperatures, in addition to increasing the processing window for with 20 mol % addition.

The reduction in modulus from adding TiO_2 at 20 mol% achieved the best match to trabecular bone with sintering at 800 °C.[40] The dissolution rate of ions was negatively impacted by adding TiO_2, though the use of DI water in this approach may not be directly representative of dissolution medium that more closely represent *in vivo* conditions due to pH and other ionic factors. The SEM/EDAX shows the formation of Ca-rich deposits on the surface of KS-0 discs rapidly, and more slowly with KS-20 discs in all pH solutions tested. There was no obvious difference between each pH at each time point.

Titanium modifies the properties of silica based bioactive glasses to better align with that of bone, though expanding on the idea for implantation and commercialization are not examined at this stage. The overshoot of adding 40 mol % $TiO_2$to a glass composition shows that there is a clearly negative mechanical and dissolution attributes that significantly reduces ionic release from these compositions, which could therefore limit its potential as a bioresorbable orthopedic material.

FUTURE WORK

To advance from this work it would be advised to take a number of routes; decreasing the TiO_2 increment, broadening the testing for biocompatibility, and producing rigid scaffolds for biocompatibility testing.

The first option would also entail finer steps for SEM imaging or ICP analysis to better understand the time points of the re-deposition from the glass to the disc surface over shorter time periods such as 12, 24, or 48 hours.

Second, the interaction of fibroblasts or osteoblast cells in cell culture, and *in vitro* testing in simulated body fluid to better understand the effect of glass dissolution, and how the addition of cations impacts the mineral deposition, and the viability of relevant cell lines.

The third approach would look more into the processing routes to develop scaffolds by traditional methods, foam replication, or additive manufacturing, robocasting. Both methods should strive to better understand the interaction with bacteria and osteoblast type cells to then enable further analysis as a bioactive material. This would also encourage the further investigation into ideal temperature for producing strong and vitreous scaffolds.

APPENDIX

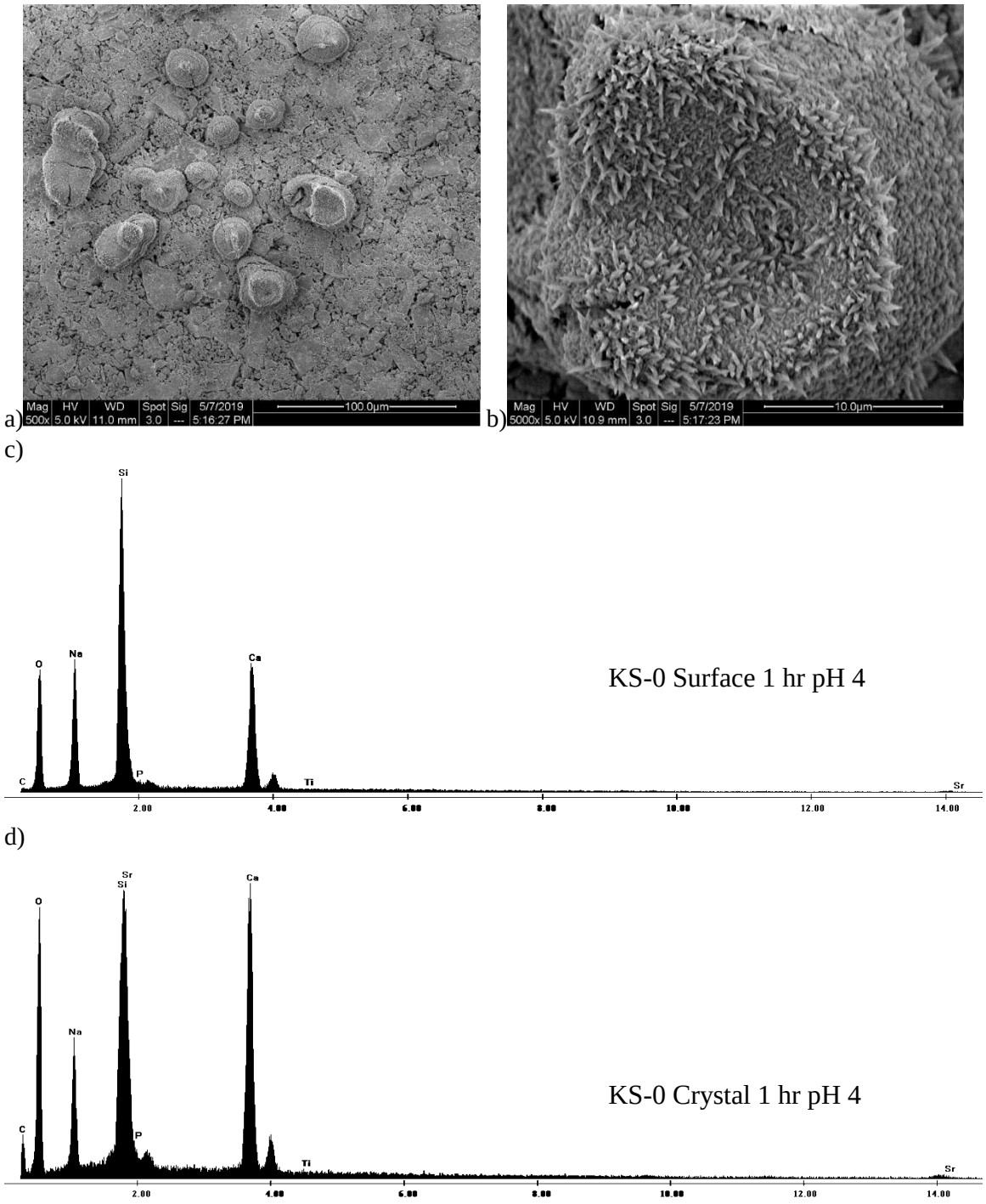

Figure 14. KS-0 1 hour pH4: a) wide view, b) crystal view, c) surface EDAX, d) crystal EDAX

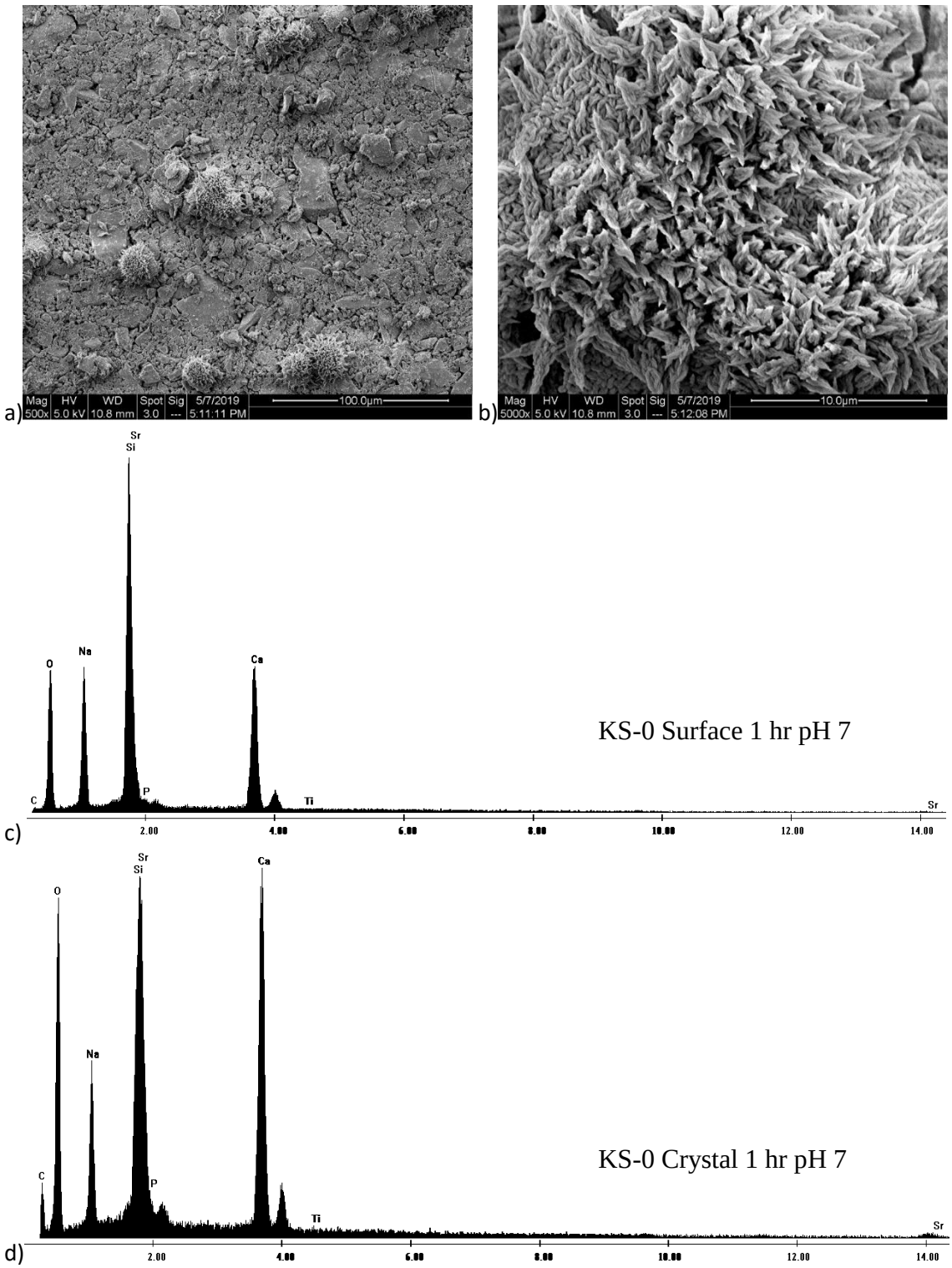

Figure 15. KS-0 1 hour pH7: a) wide view, b) crystal view, c) surface EDAX, d) crystal EDAX

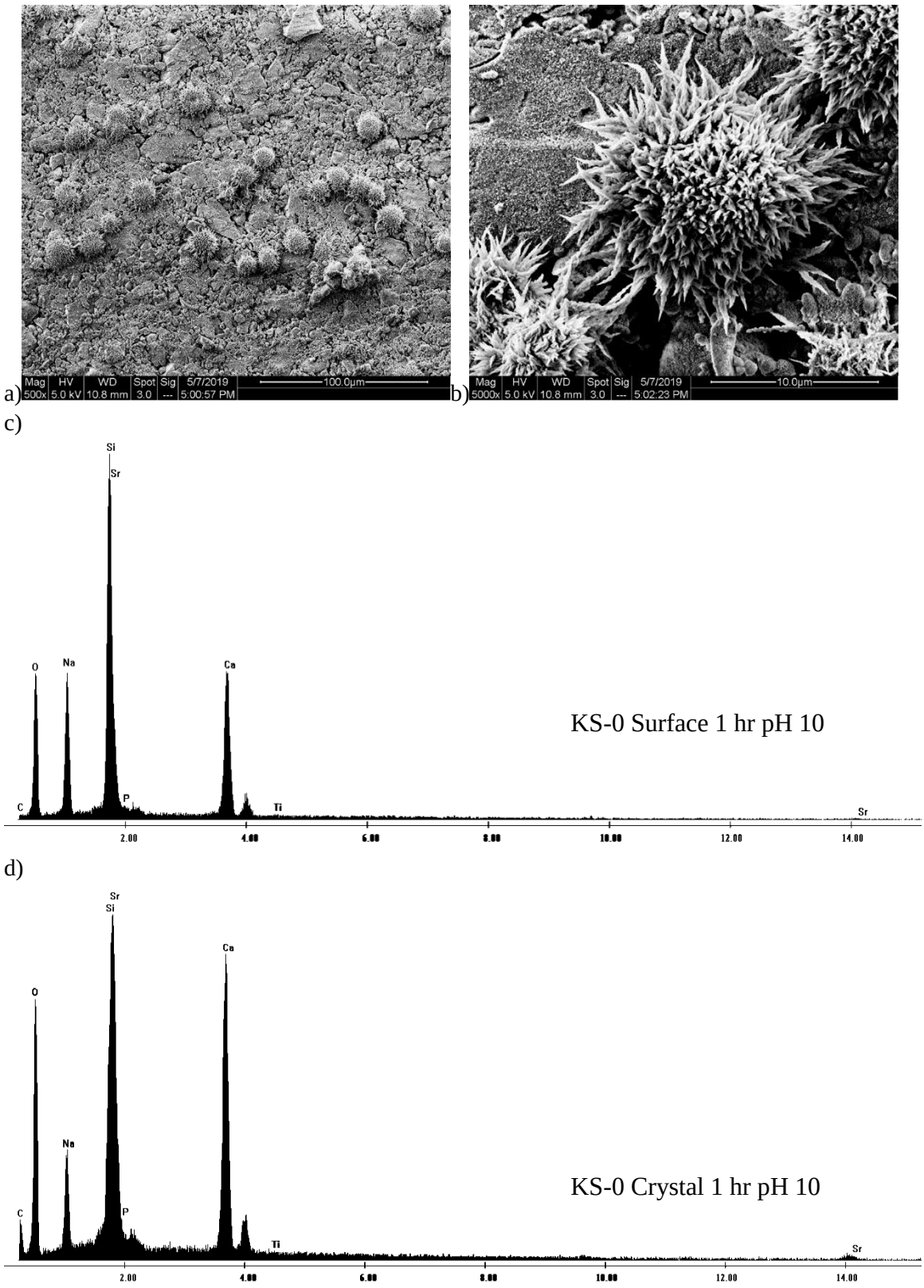

Figure 16. KS-0 1 hour pH10: a) wide view, b) crystal view, c) surface EDAX, d) crystal EDAX

a) 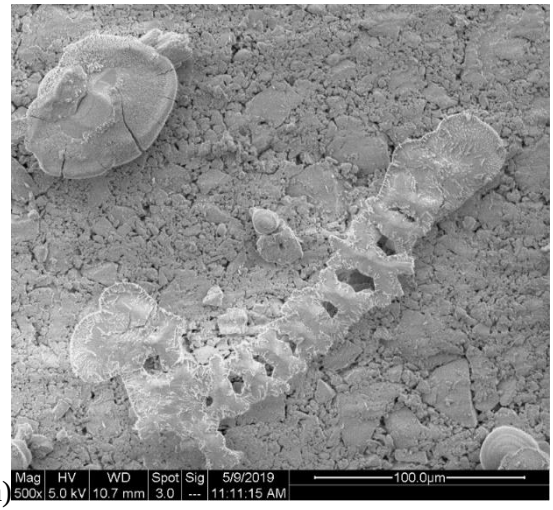

b) 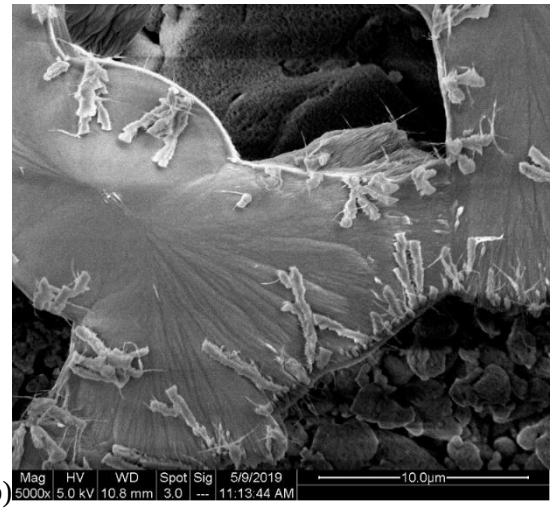

c) 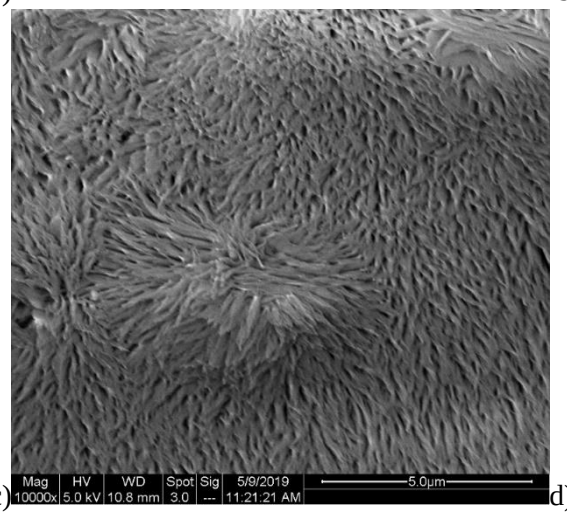

d) 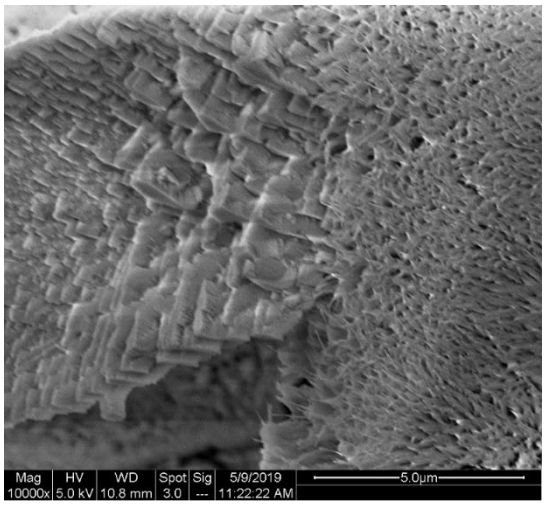

e)

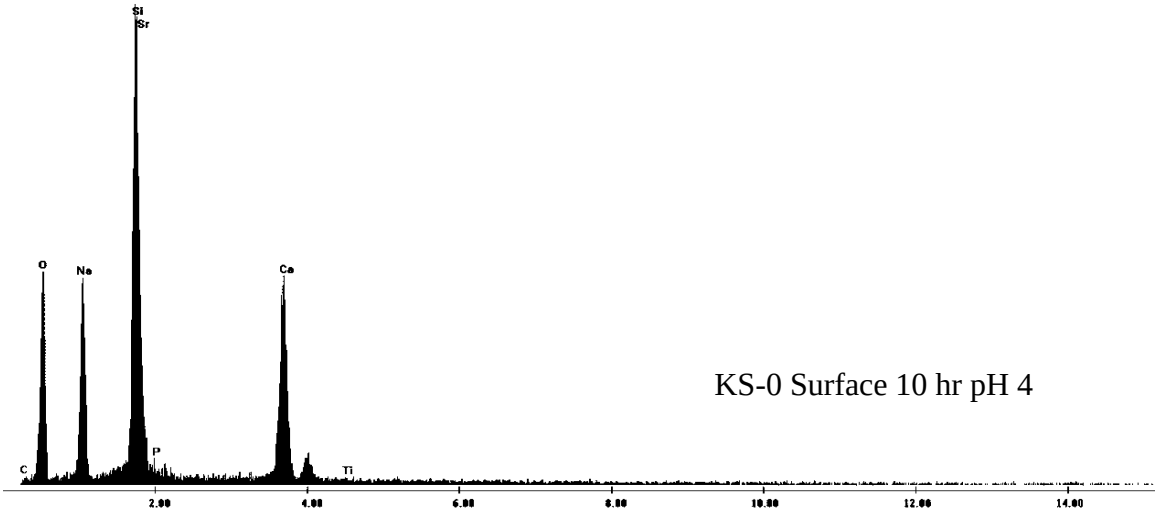

KS-0 Surface 10 hr pH 4

f)

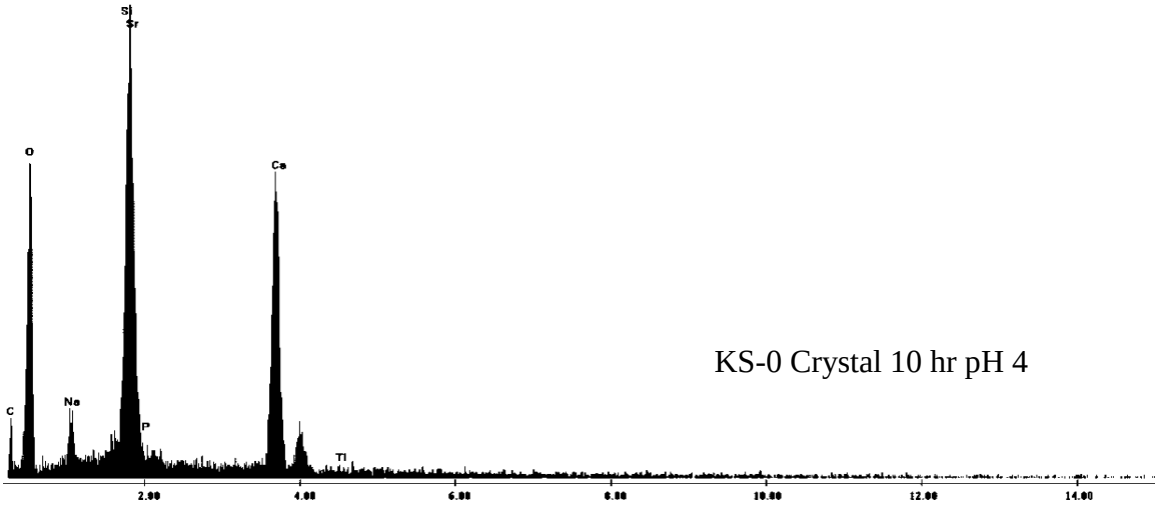

Figure 17. KS-0 10 hr pH 4: a) wide view, b) close view of dendrite, c) hair-like protrusions on collapsed sphere, d) plate-like structure growth, e) EDAX of surface(dendtride is similar and not shown) , f) EDAX of crystal in c and d

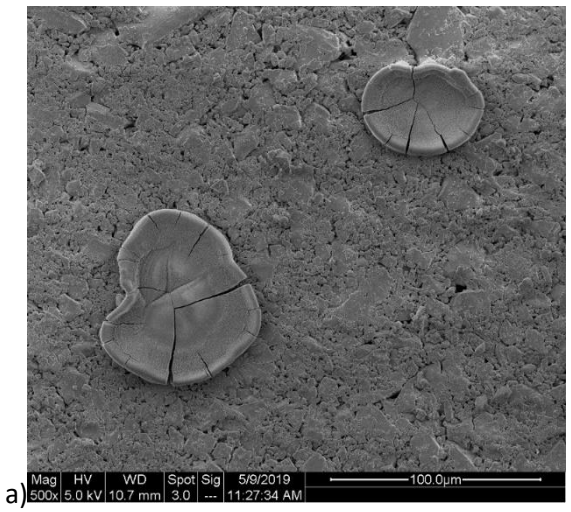

a)

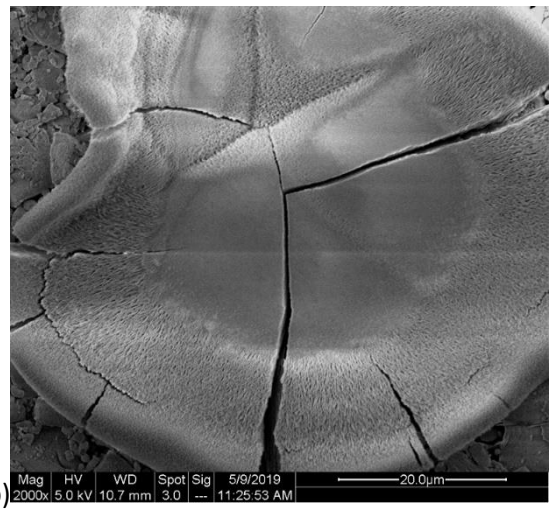

b)

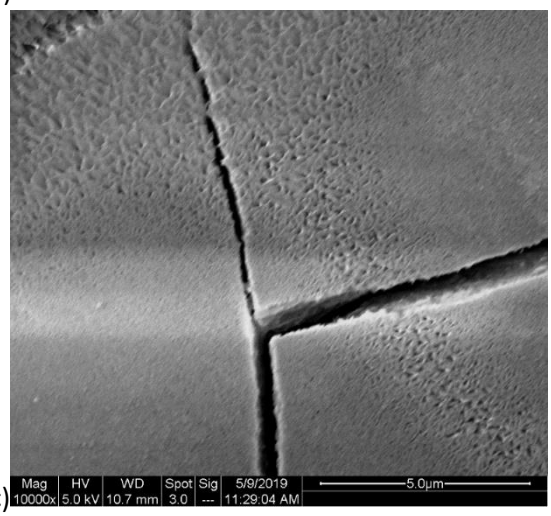

c)

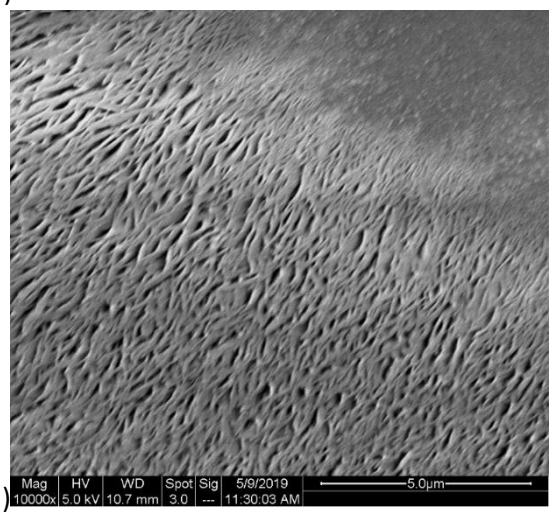

d)

e)

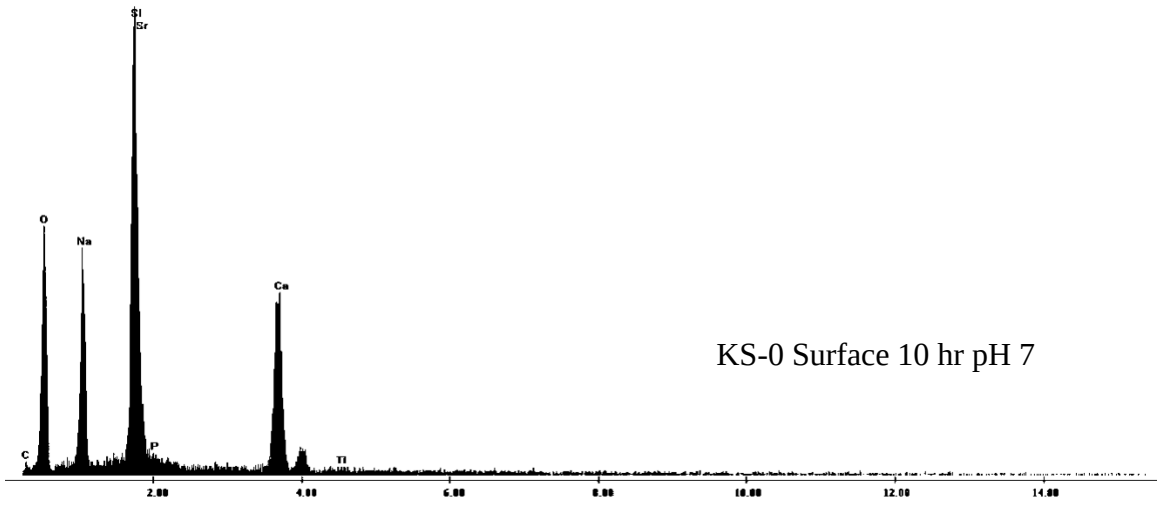

KS-0 Surface 10 hr pH 7

f)

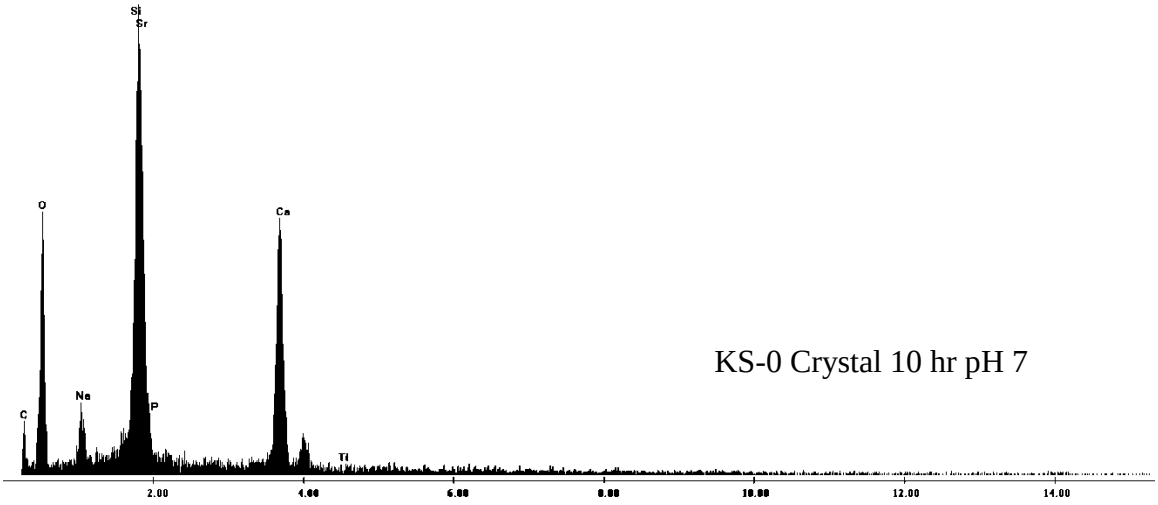

Figure 18. KS-0 10 hr pH 7: a) wide view, b) close view of sphere, c) further image of sphere, d) hair-like protrusions on collapsed sphere, e) EDAX of surface, f) EDAX of sphere

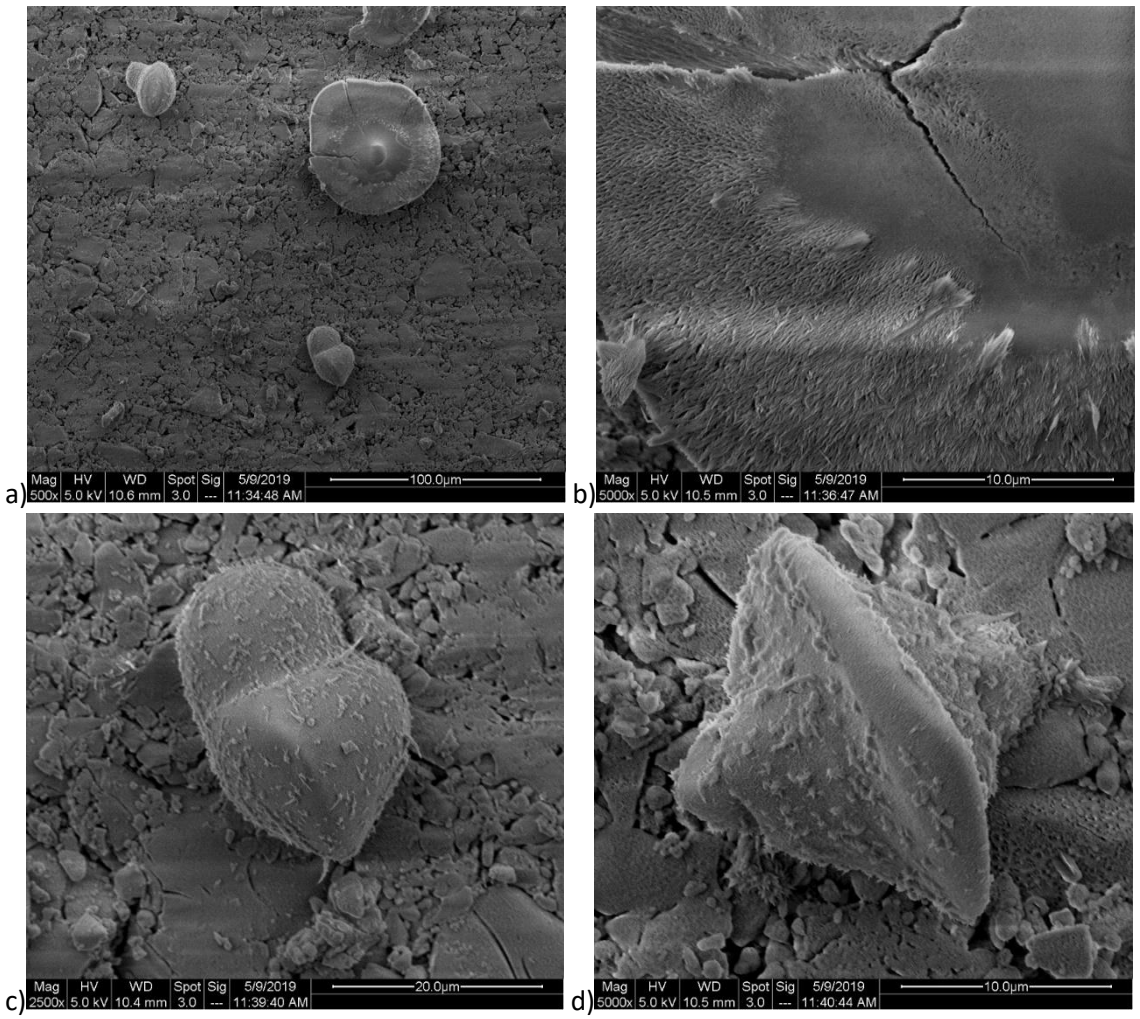

e)

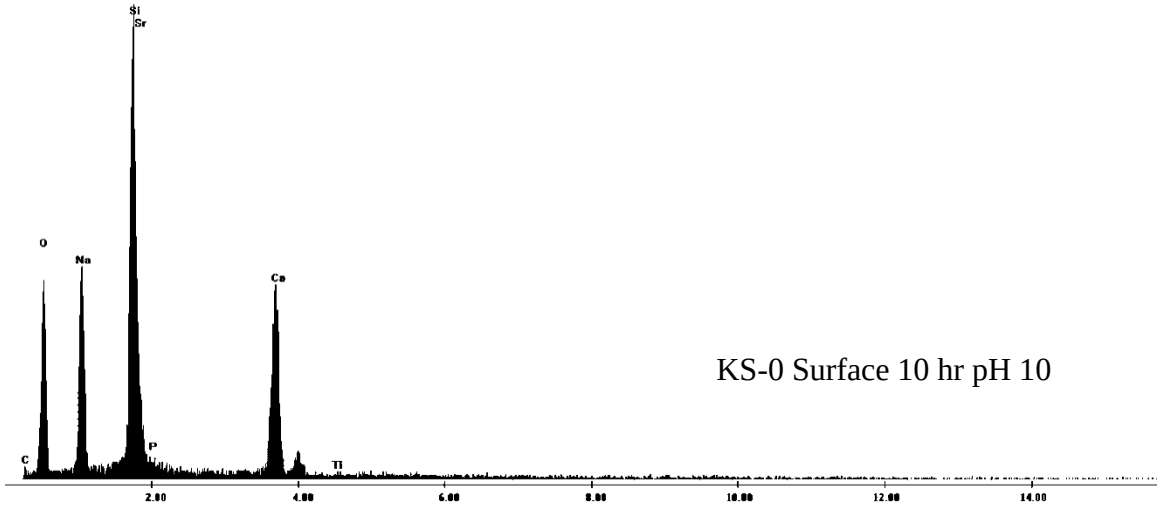

KS-0 Surface 10 hr pH 10

f)

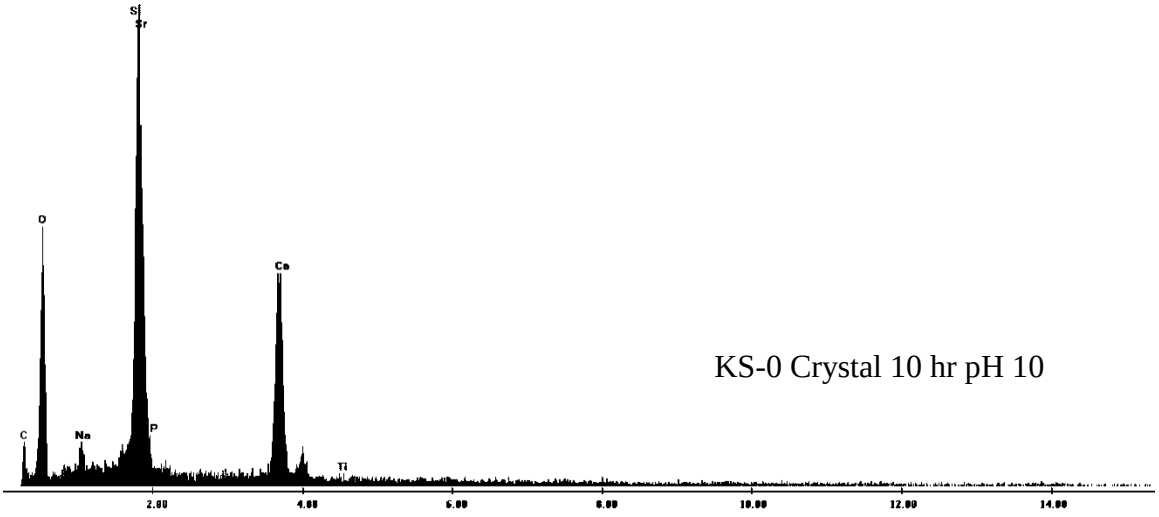

Figure 19. KS-0 10 hr pH 10: a) wide view, b) close view of sphere, c) surface feature, d) hair-like protrusions on collapsed sphere, e) EDAX of surface, f) EDAX of sphere

a)

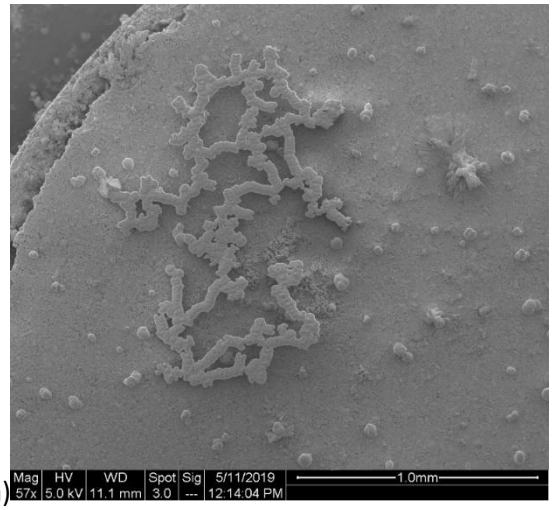

b)

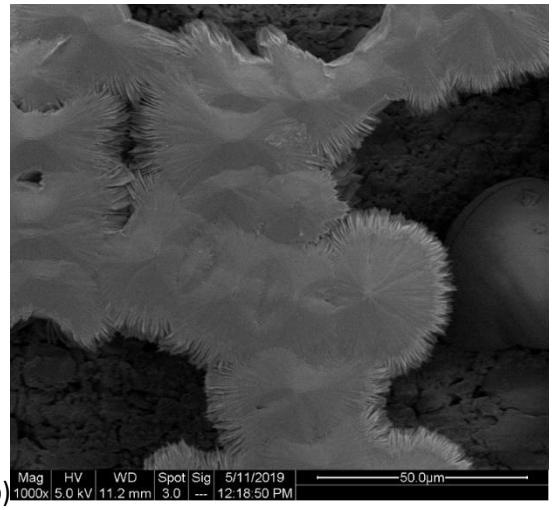

c)

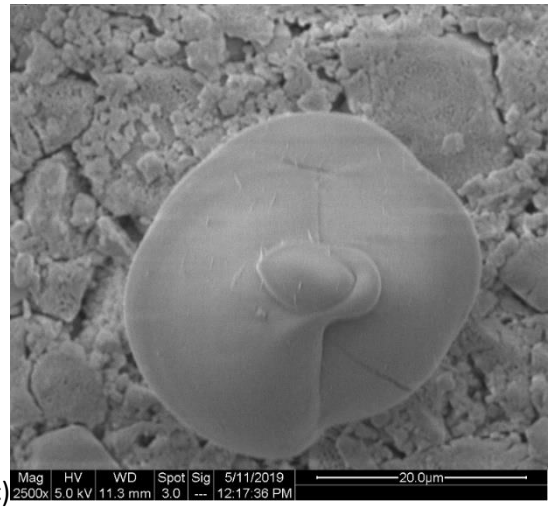

d)

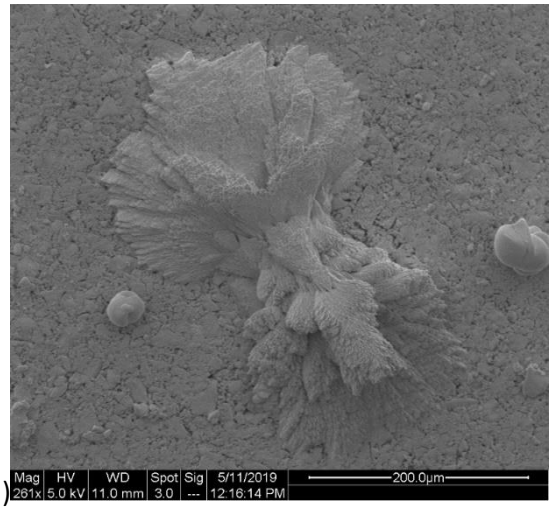

e)

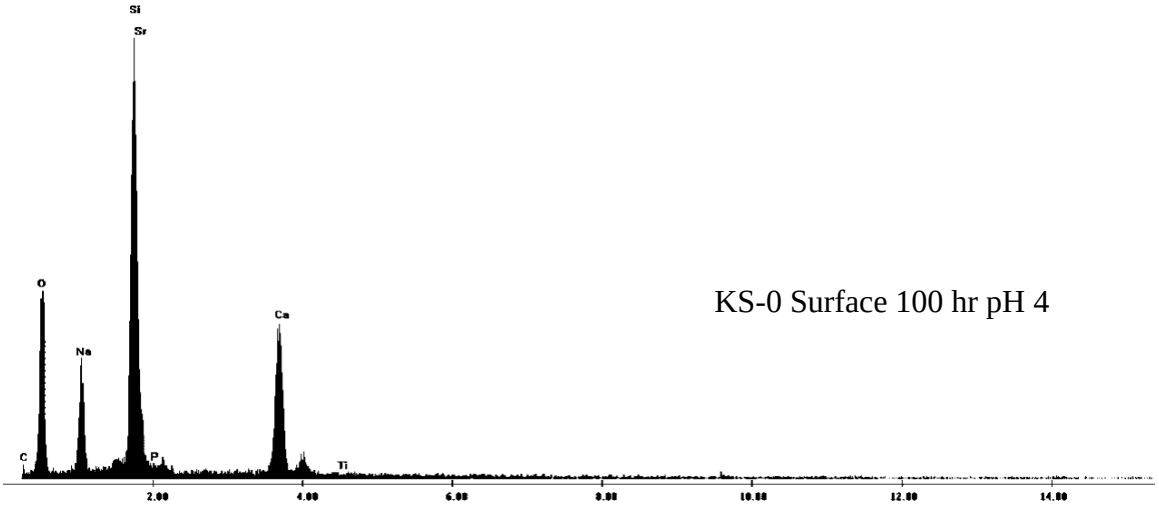

KS-0 Surface 100 hr pH 4

f)

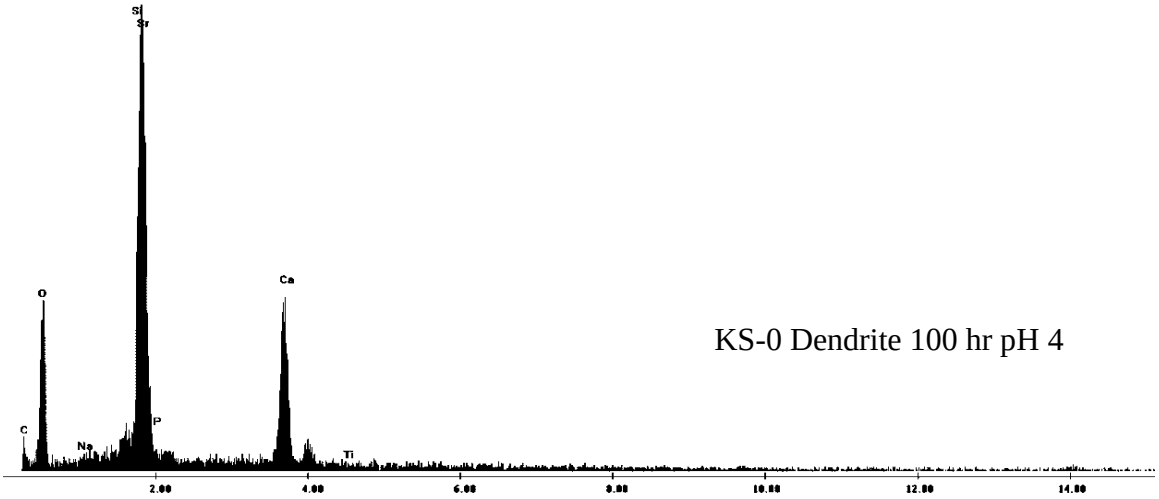

g)

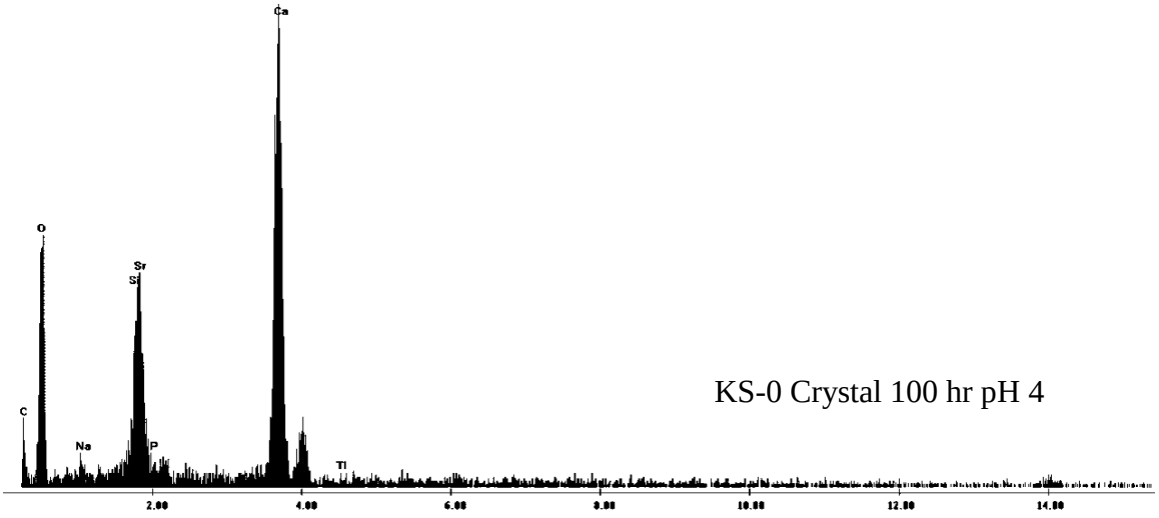

Figure 20. KS-0 100 hr pH 4: a) wide view, b) close view of dendrite, c) view of spherical deposit, d) flower-like growth, e) EDAX of surface, f) EDAX of dendrite, g) EDAX of crystal

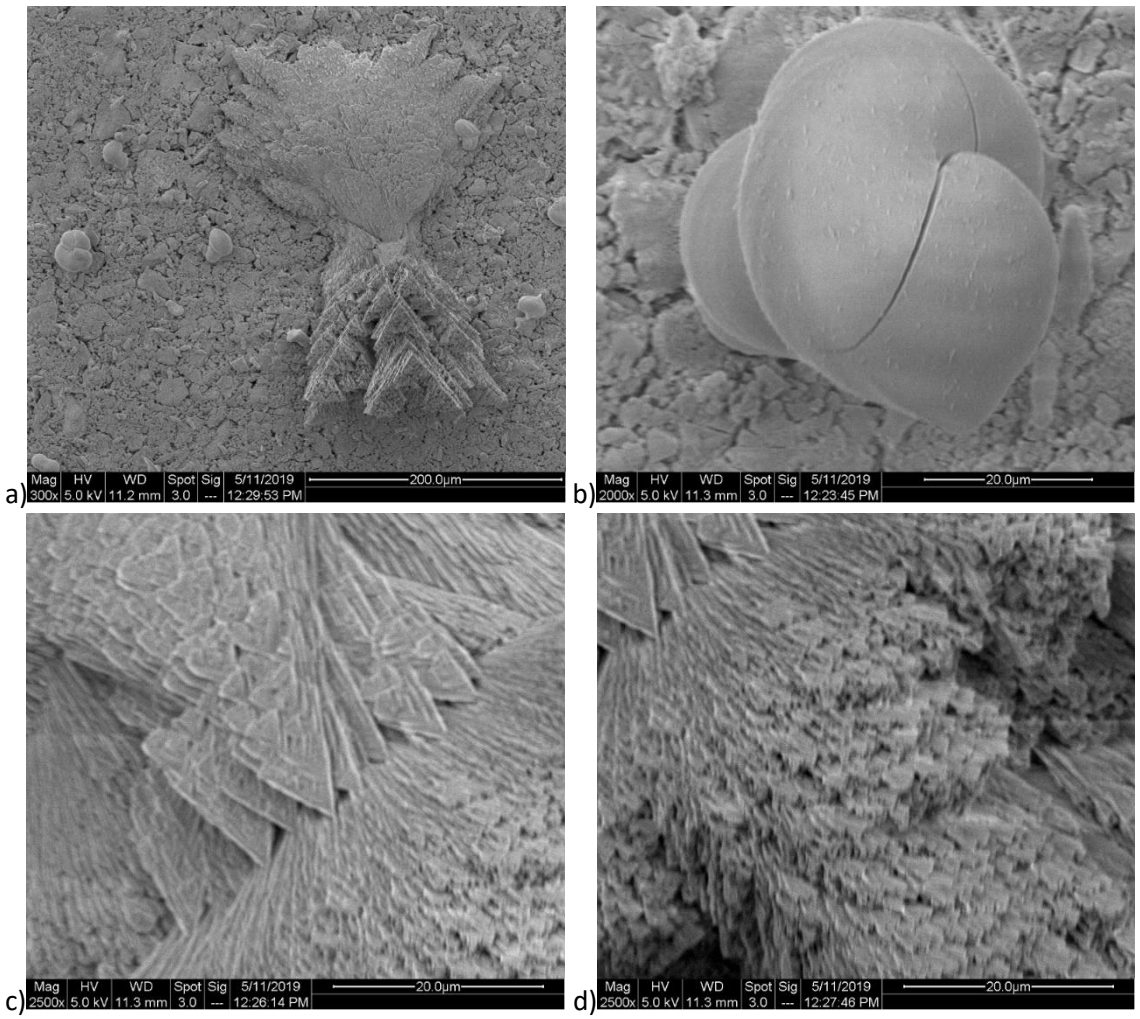

e)

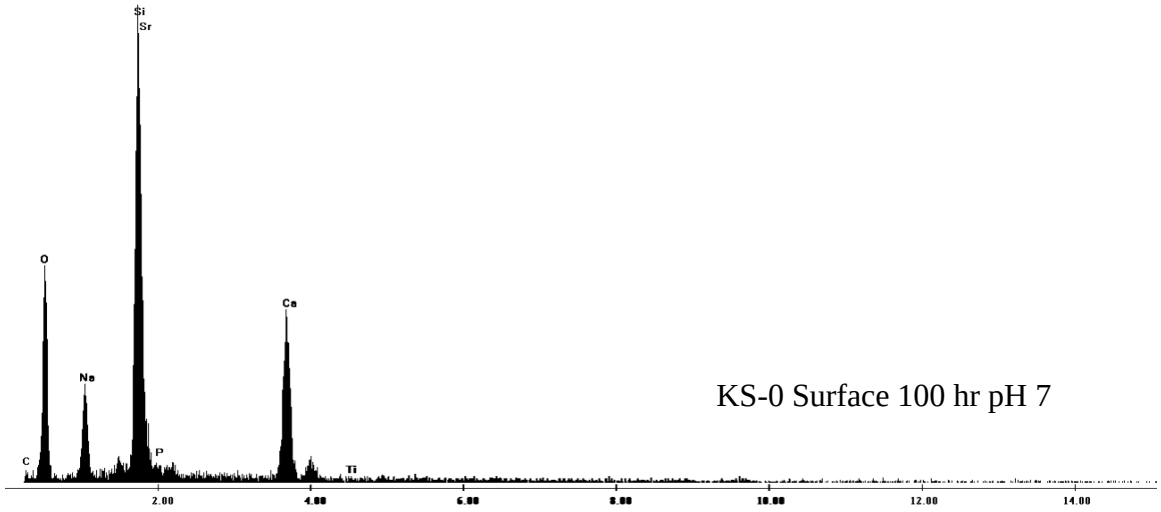

KS-0 Surface 100 hr pH 7

f)

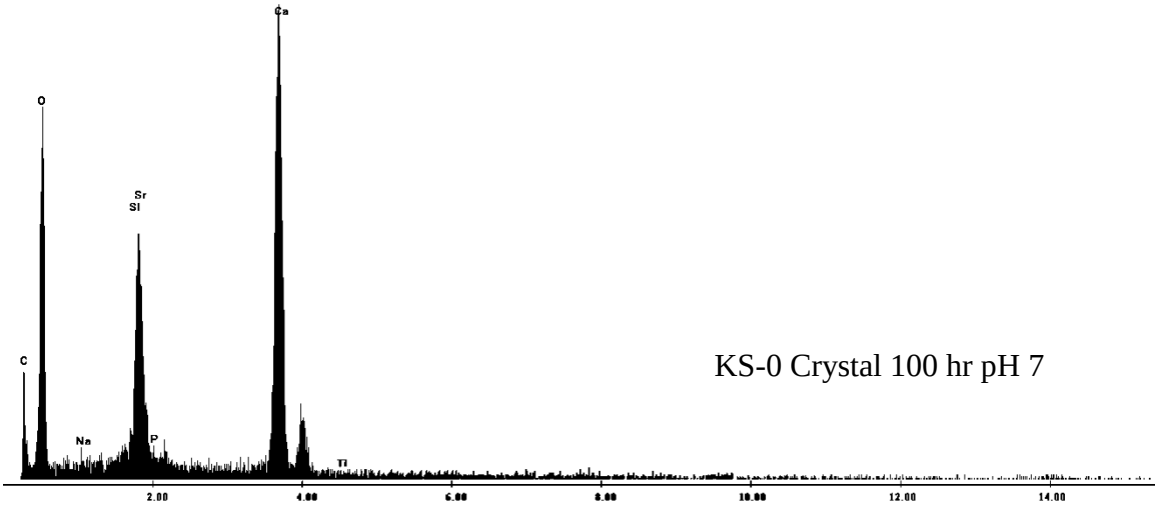

Figure 21. KS-0 100 hr pH 7: a) wide view, b) close view of sphere, c) closer image of crystal, d), e) EDAX of surface, f) EDAX of crystal

a)

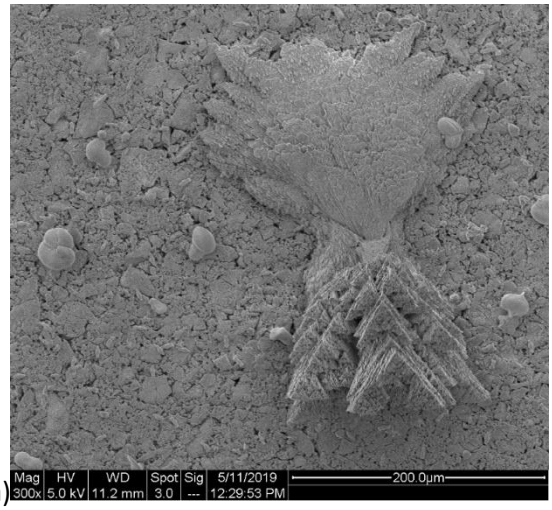

b)

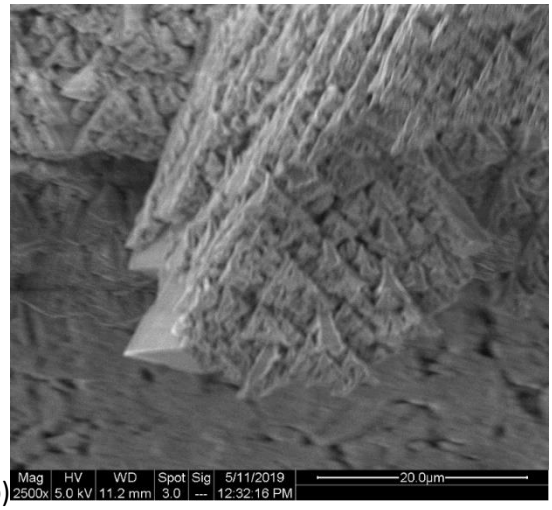

c)

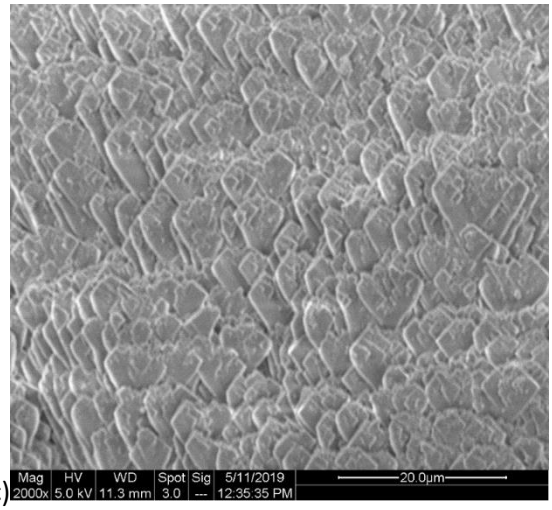

d)

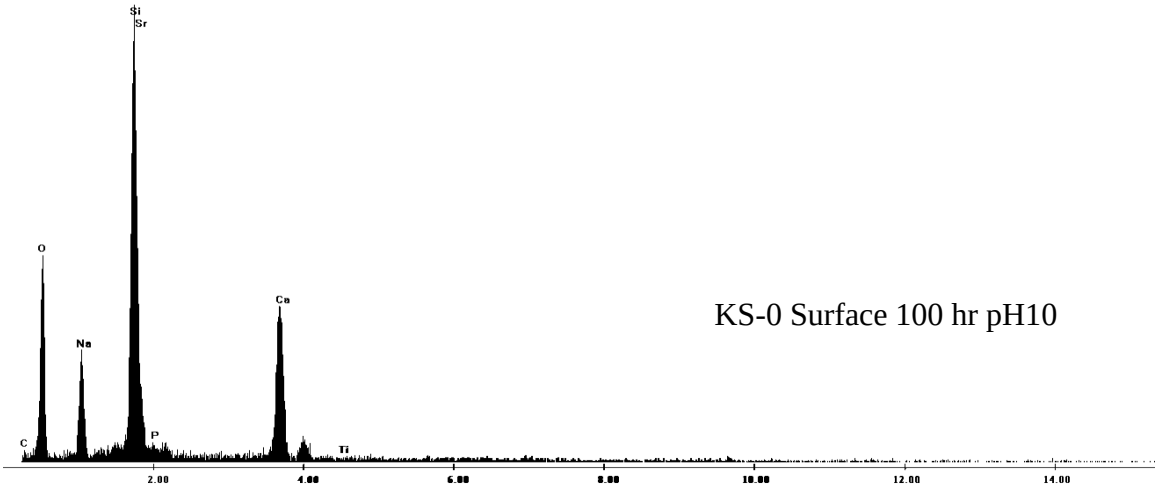

KS-0 Surface 100 hr pH10

e)

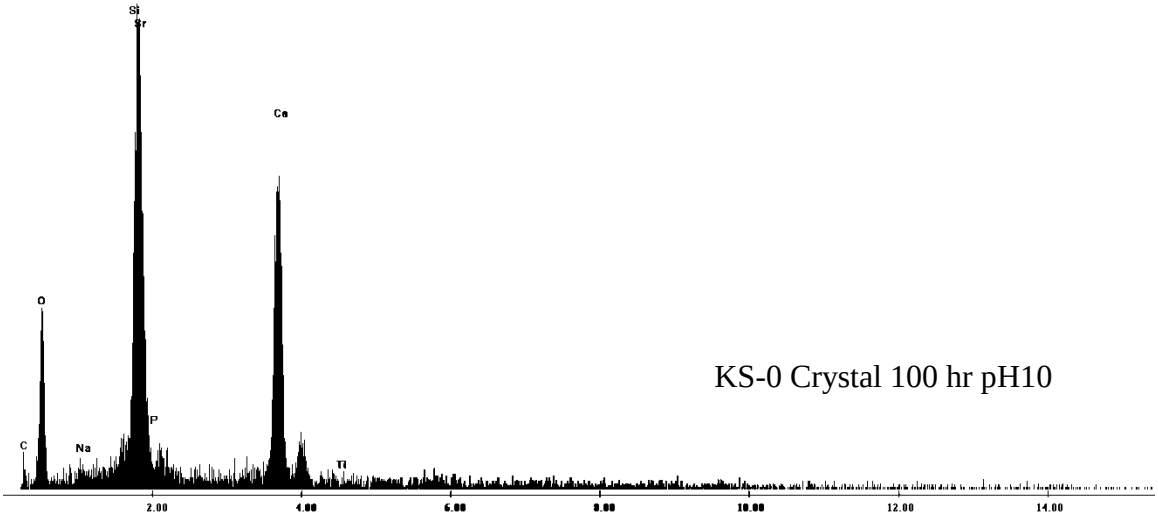

Figure 22. KS-0 100 hr pH 10: a) wide view, b) close view of crystal, c) image of upper half of the crystal, d) EDAX of surface, e) EDAX of crystal

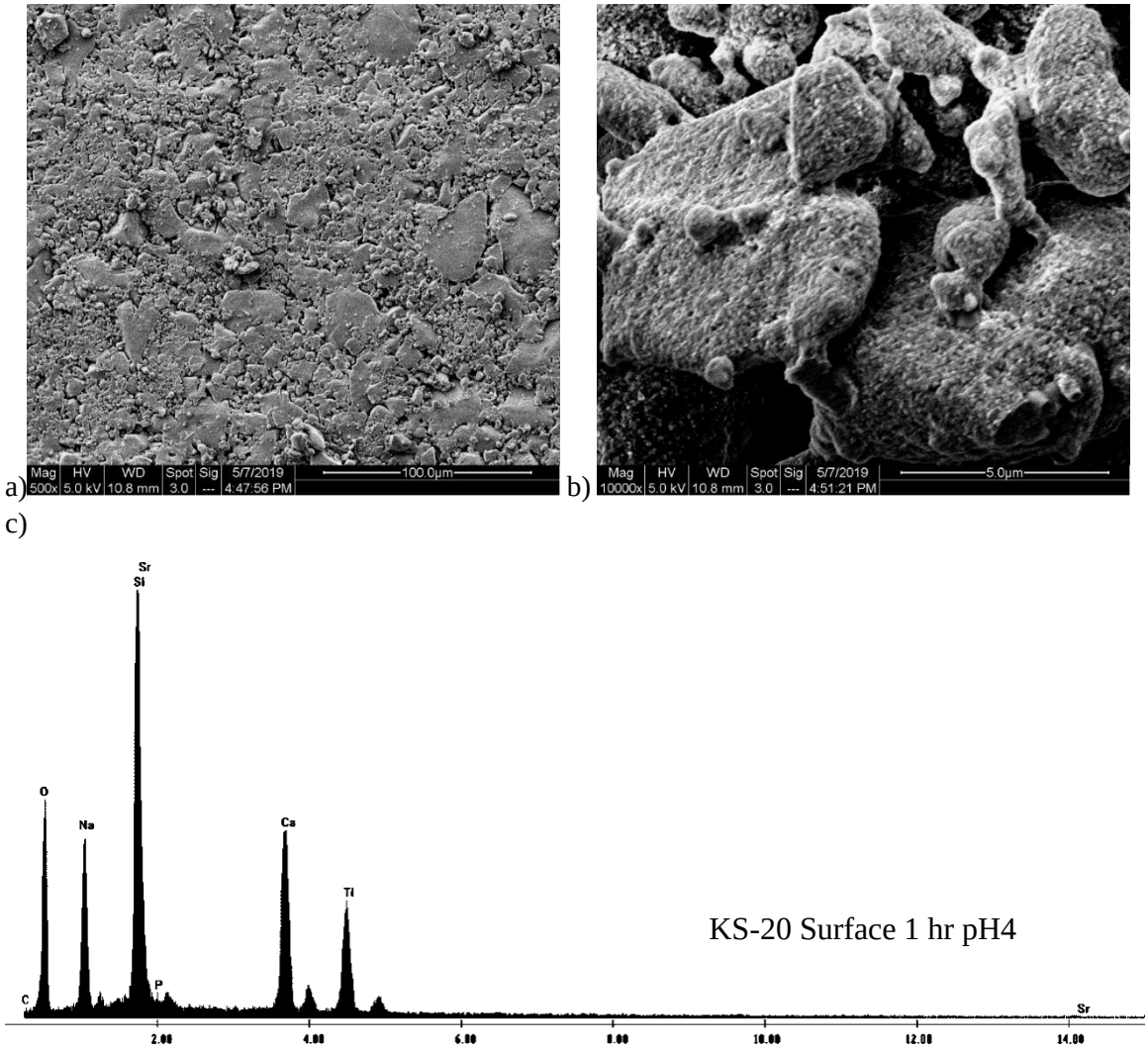

Figure 23. KS-20 1 hr pH 4: a) wide view, b) close view, c) surface EDAX

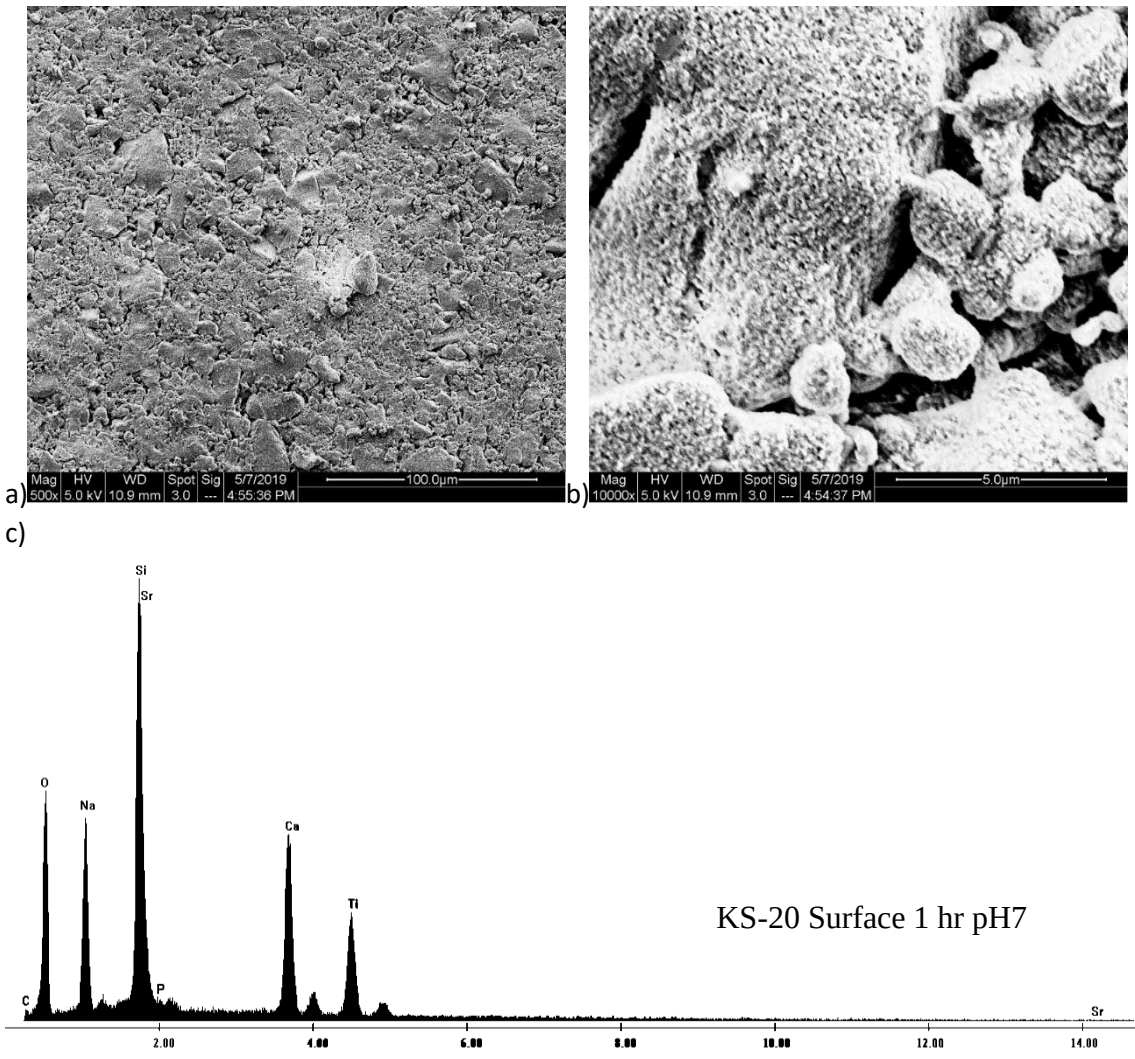

Figure 24. KS-20 1 hr pH 7: a) wide view, b) close view, c) surface EDAX

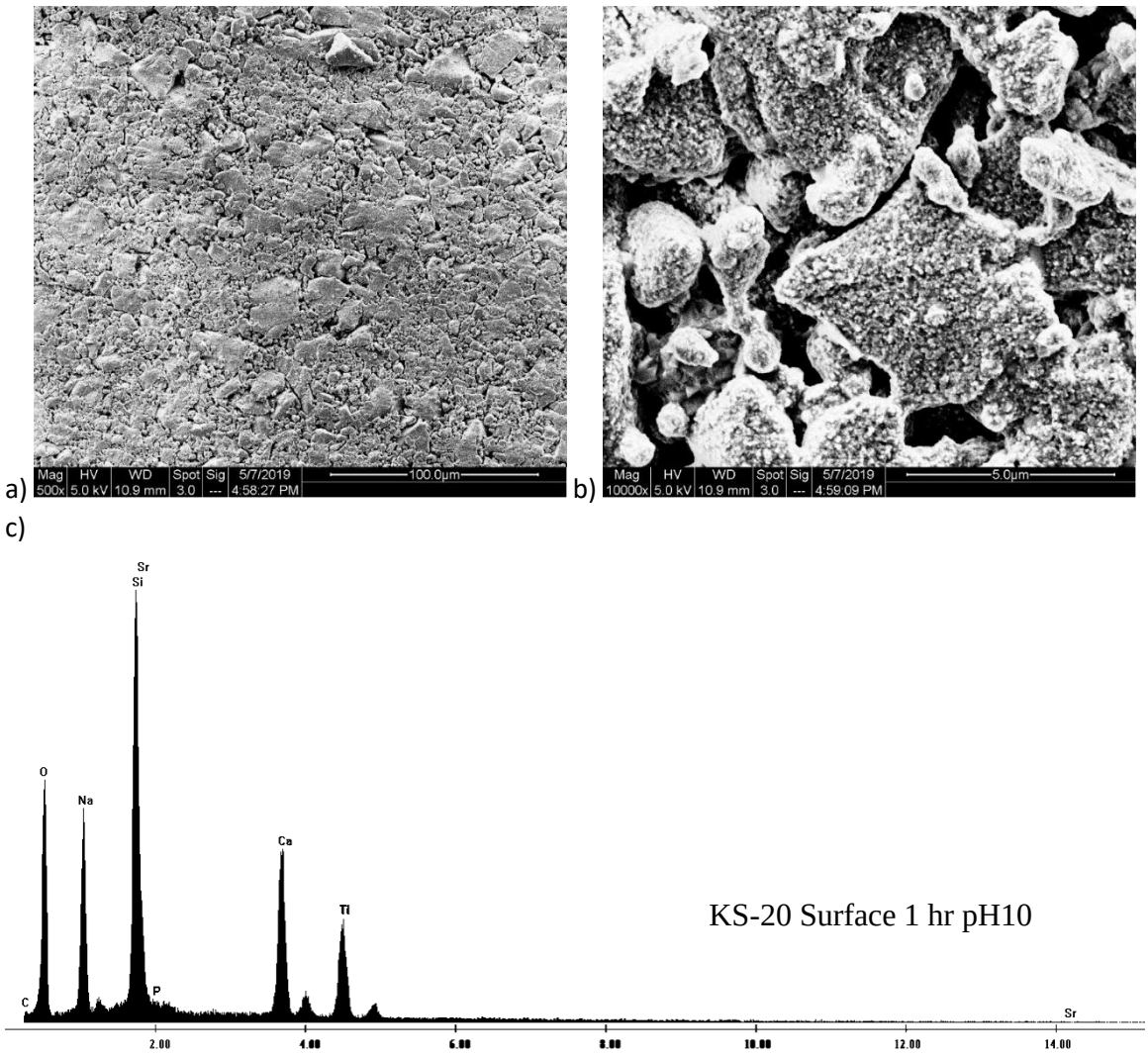

Figure 25. KS-20 1 hr pH 10: a) wide view, b) close view of pitting, c) EDAX of surface

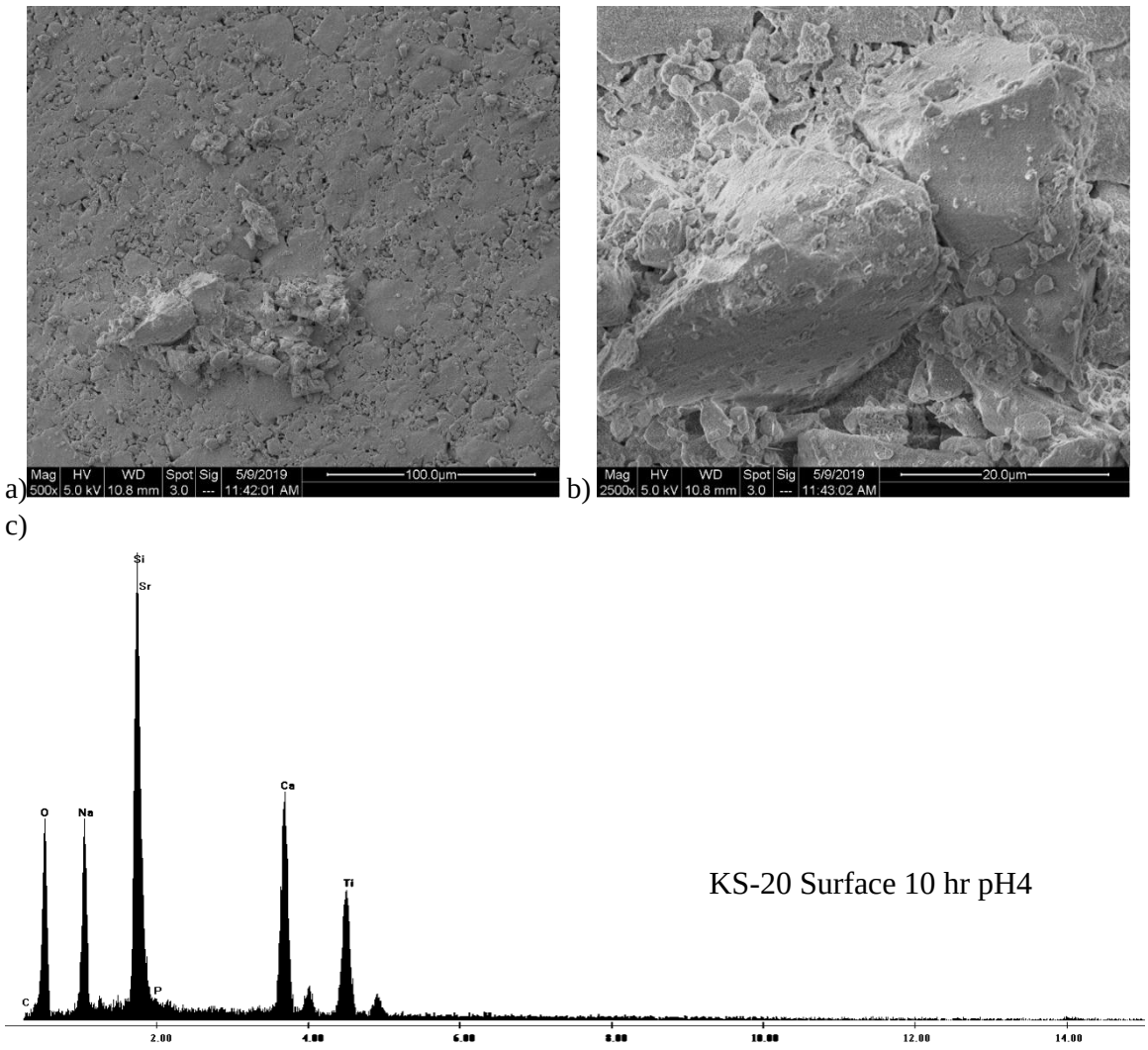

Figure 26. KS-20 10 hr pH 4: a) wide surface view, b) closer examination of crystal, c) EDAX of surface, d) EDAX of crystal

a)

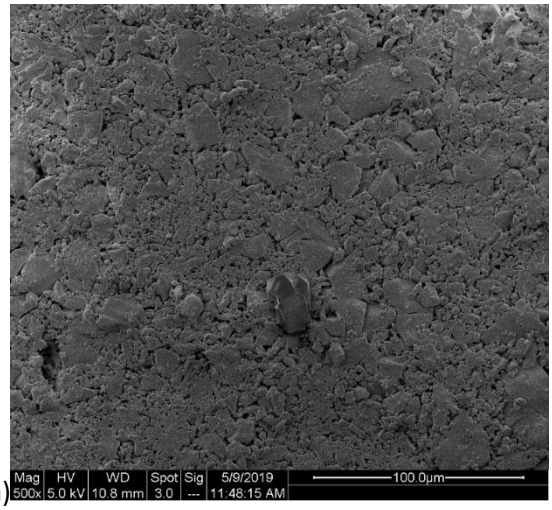

b)

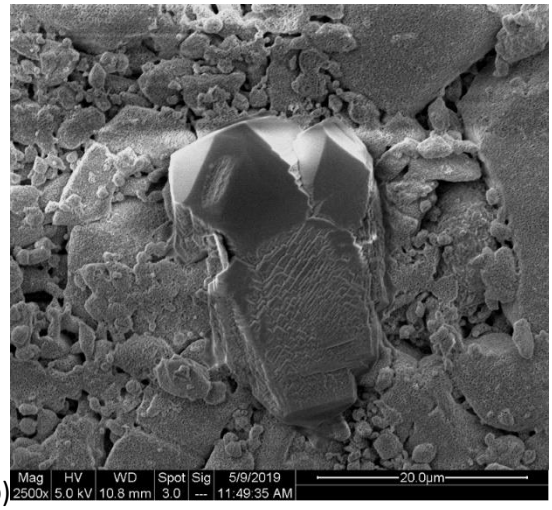

c)

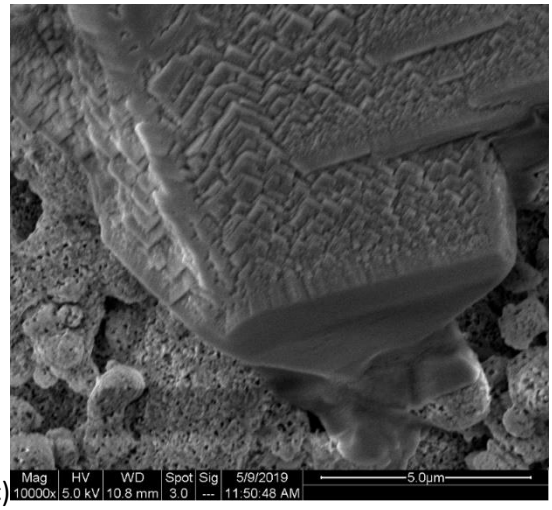

d)

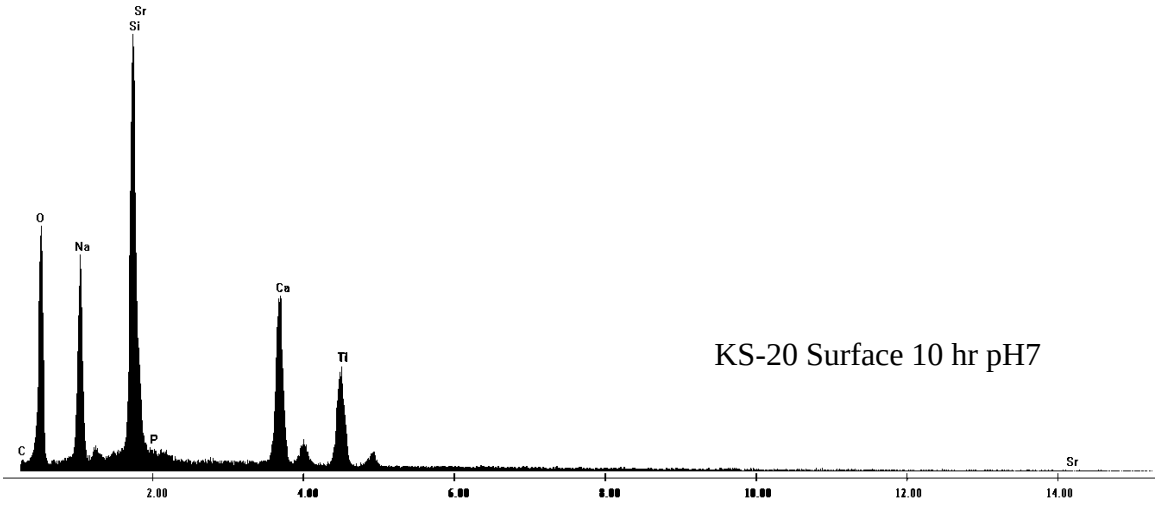

KS-20 Surface 10 hr pH7

e)

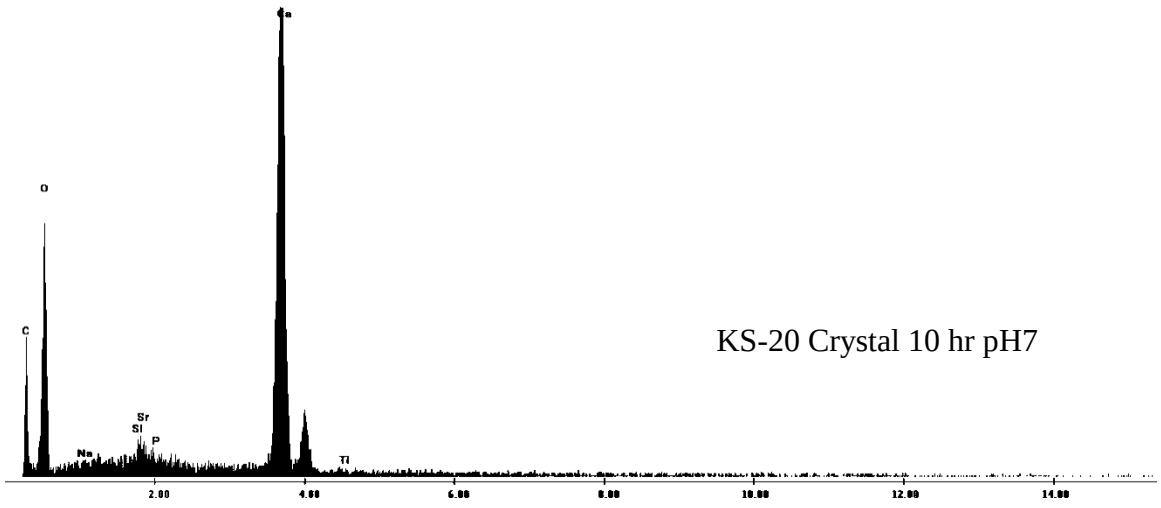

Figure 27. KS-20 10 hr pH 7: a) wide surface view, b) closer examination of crystal, c) examination of crystal anchoring, d) EDAX of surface, e) EDAX of crystal

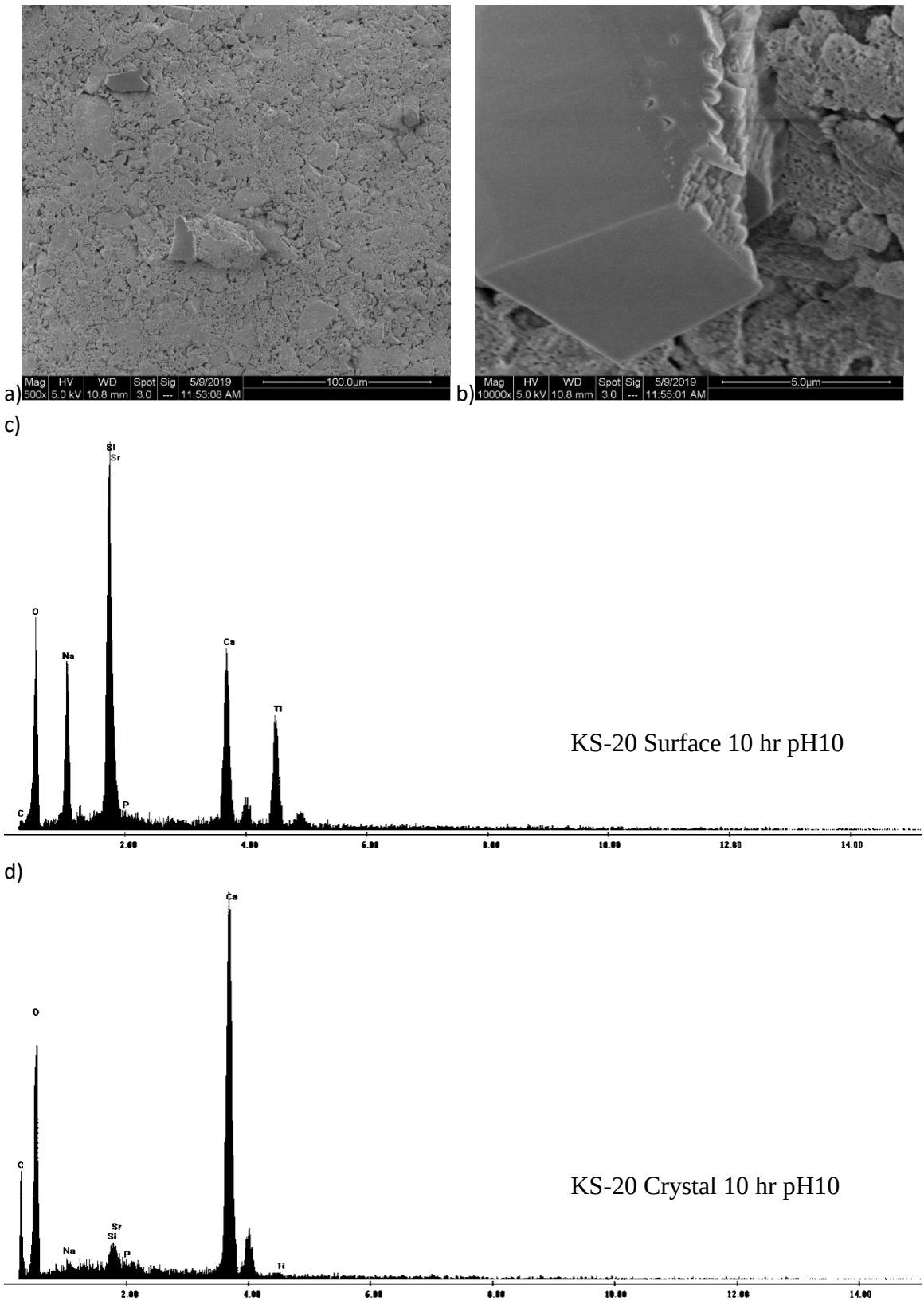

Figure 28. KS-20 10 hr pH 10: a) wide surface view, b) crystal view, c) EDAX of surface, d) EDAX of crystal

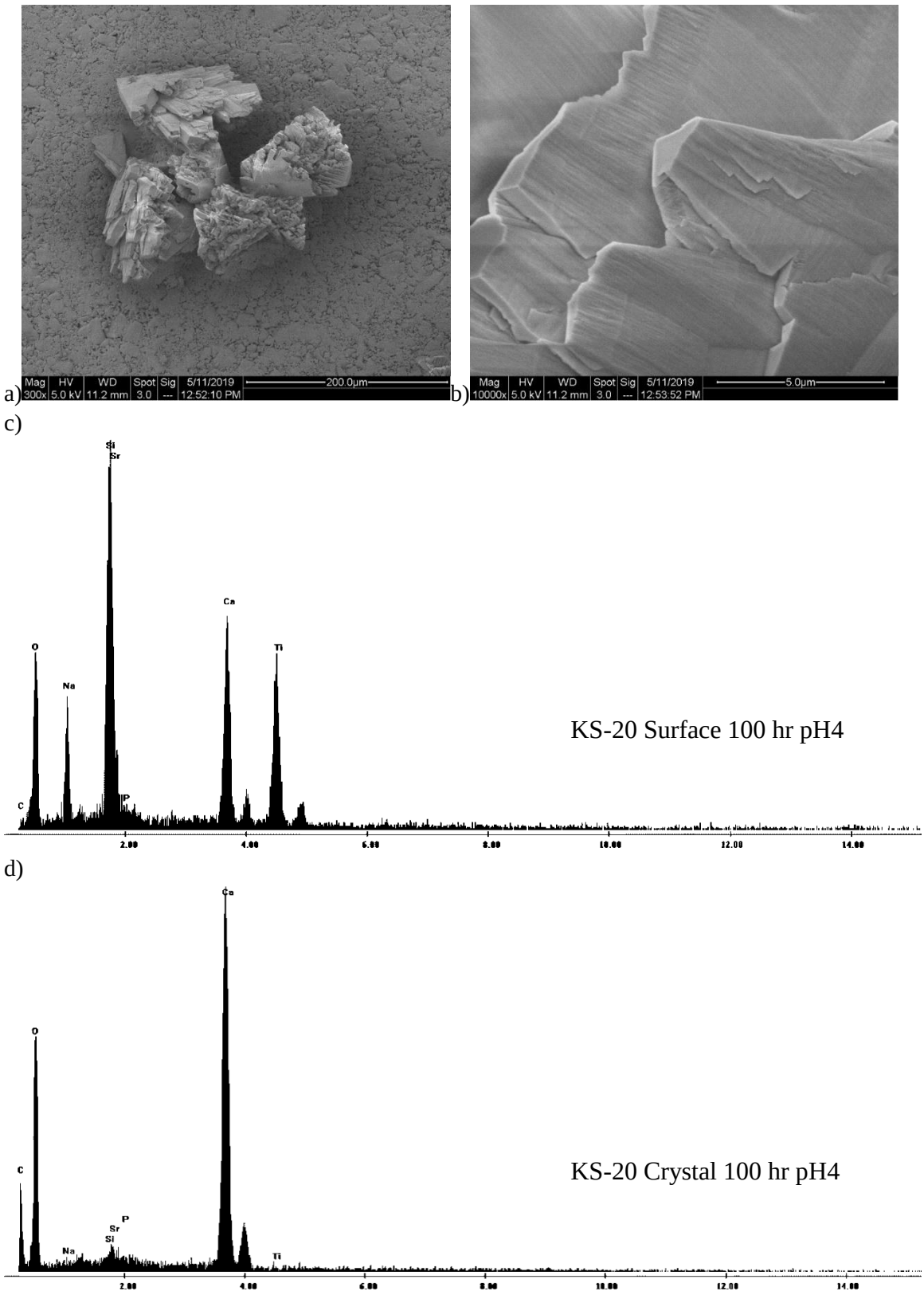

Figure 29. KS-20 100 hr pH 4: a) broad surface view, b) closer view of crystal, c) EDAX of surface, d) EDAX of crystal

a) 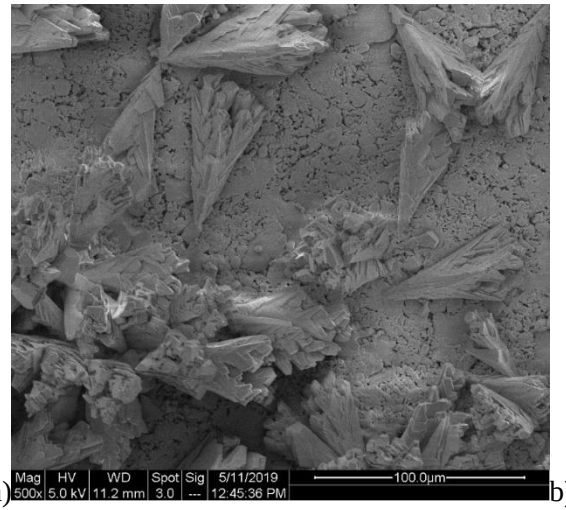

b) 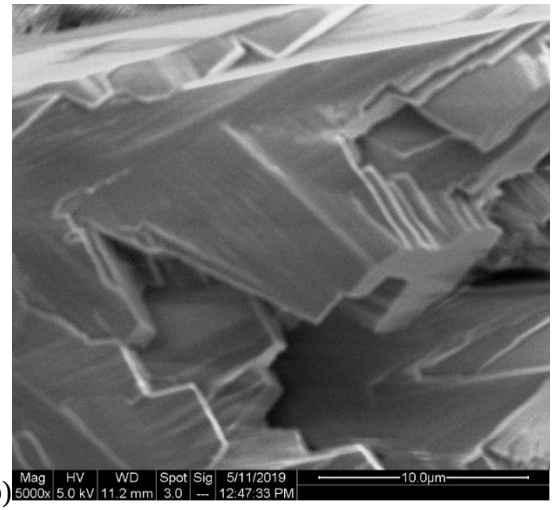

c) 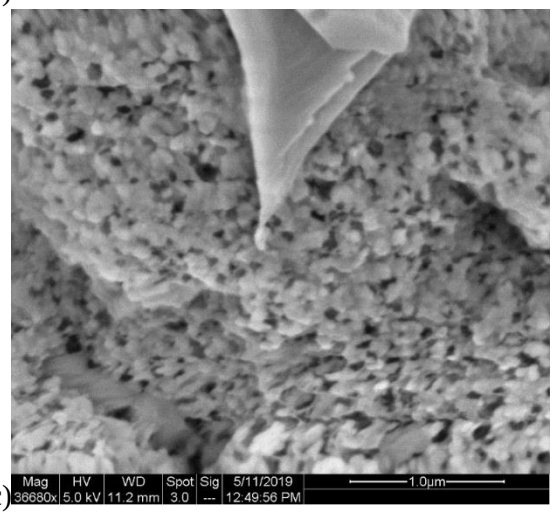

d) 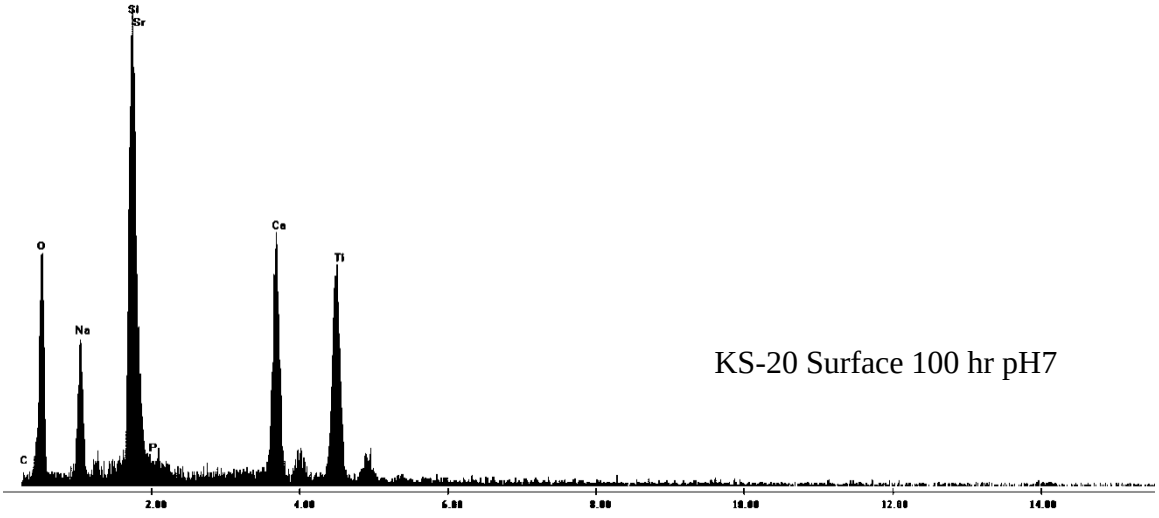

KS-20 Surface 100 hr pH7

e)

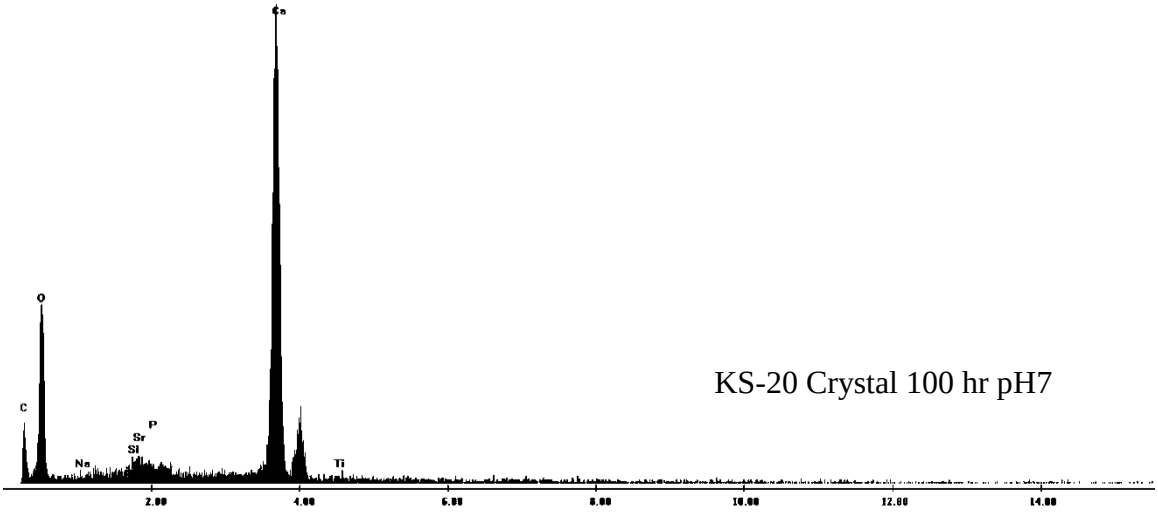

Figure 30. KS-20 100 hr pH 7: a) broad surface view, b) closer view of crystal, c) crystal attachment to the disc surface, d) EDAX of surface, e) EDAX of the crystal

a) 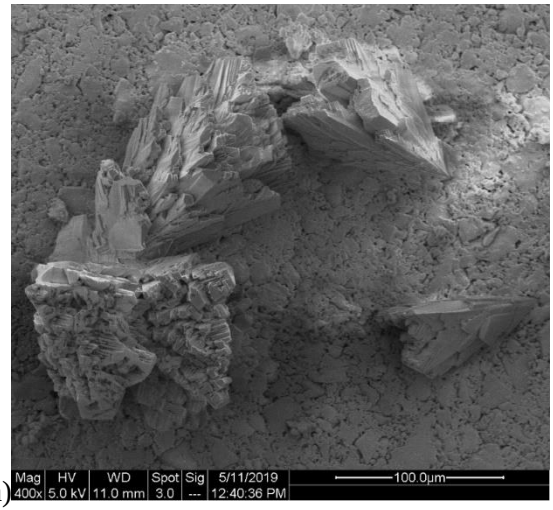
Mag HV WD Spot Sig 5/11/2019
400x 5.0 kV 11.0 mm 3.0 --- 12:40:36 PM
100.0µm

b) 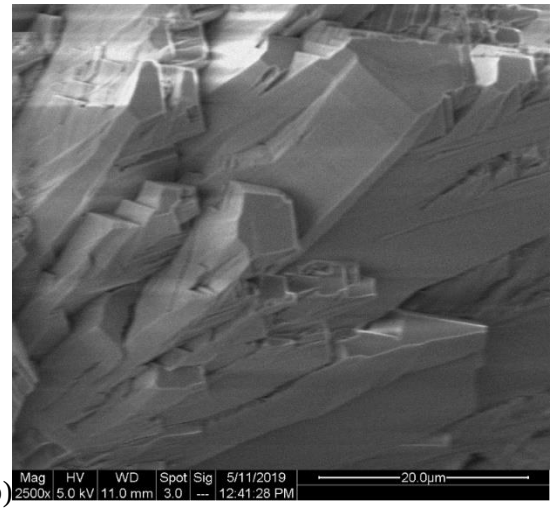
Mag HV WD Spot Sig 5/11/2019
2500x 5.0 kV 11.0 mm 3.0 --- 12:41:28 PM
20.0µm

c) 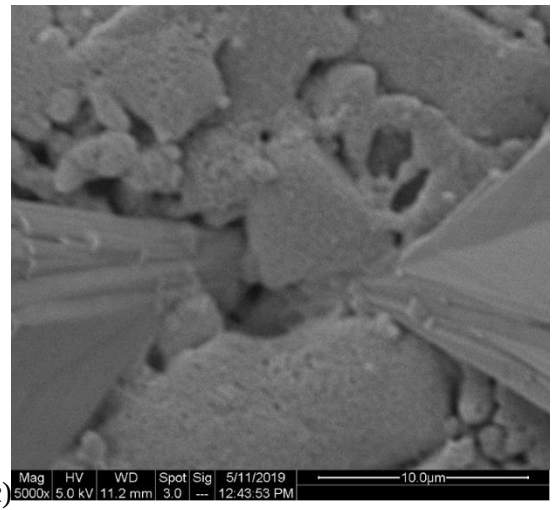
Mag HV WD Spot Sig 5/11/2019
5000x 5.0 kV 11.2 mm 3.0 --- 12:43:53 PM
10.0µm

d)

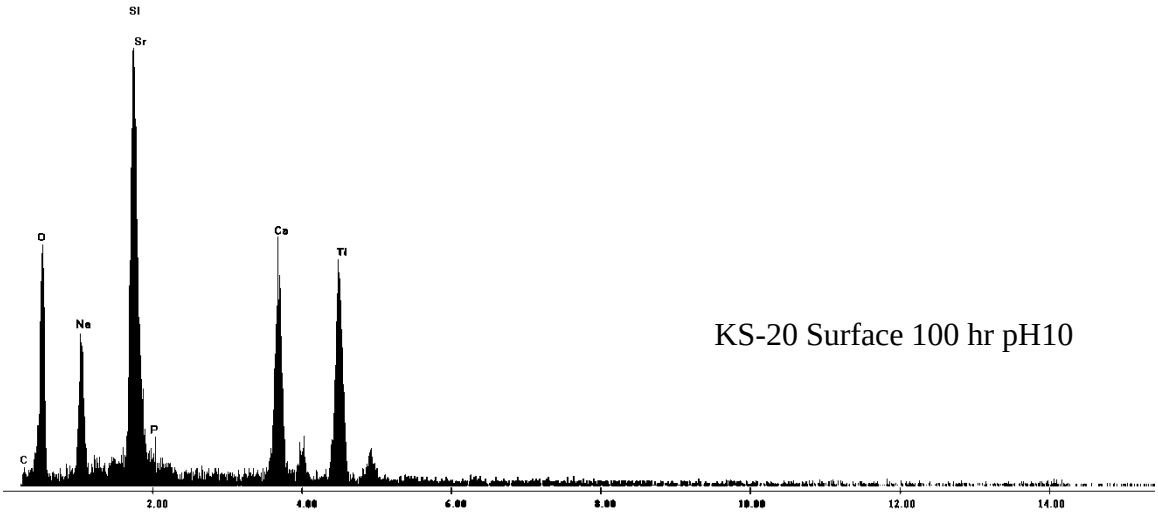

e)

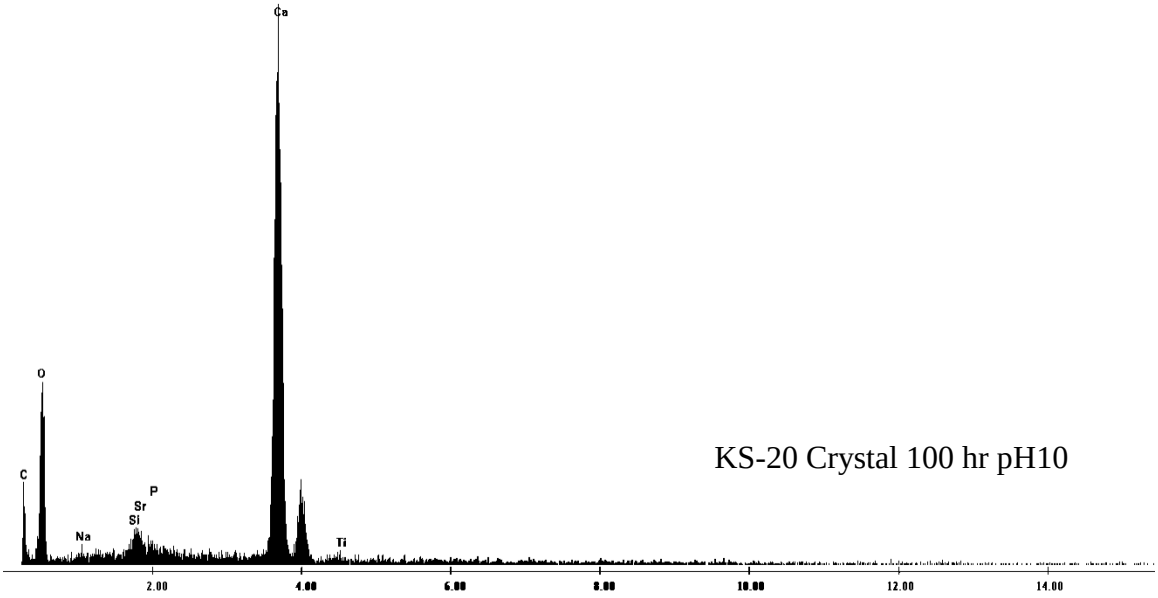

Figure 31. KS-20 100 hr pH 10: a) broad surface view, b) closer view of crystal, c) crystal attachment to the disc surface, d) EDAX of surface, e) EDAX of the crystal

REFERENCES

1. L. G. Donaruma, "Definitions in Biomaterials, D. F. Williams, Ed., Elsevier, Amsterdam, 1987, 72 Pp," *J. Polym. Sci., Part C: Polym. Lett.,* **26** [9] 414 (1988).

2. W. Jin and P. K. Chu, "Orthopedic Implants"; pp. 425-39 in *Encycl. Biomater. Biomed. Eng.* Edited by R. Narayan. Elsevier, Oxford, 2019.

3. H. Zhou, M. Jiang, Y. Xin, G. Sun, S. Long, S. Bao, X. Cao, S. Ji, and P. Jin, "Surface Deposition of Graphene Layer for Bioactivity Improvement of Biomedical 316 Stainless Steel," *Mater. Lett.*, **192,** 123-7 (2017).

4. A. García-Argumánez, I. Llorente, O. Caballero-Calero, Z. González, R. Menéndez, M. L. Escudero, and M. C. García-Alonso, "Electrochemical Reduction of Graphene Oxide on Biomedical Grade CoCr Alloy," *Appl. Surf. Sci.*, **465,** 1028-36 (2019).

5. F. E. A. Bandyopadhyay, V. K. Balla, S. Bose, Y. Ohgami, N. M. Davies, "Influence of Porosity on Mechanical Properties and in Vivo Response of Ti6Al4V Implants," *Acta Biomater.,* **6** [4] 1640-8 (2010).

6. Q.-H. Zhang, A. Cossey, and J. Tong, "Stress Shielding in Bone of a Bone-Cement Interface," *Med. Eng. Phys.*, **38** [4] 423-6 (2016).

7. M. Geetha, A. K. Singh, R. Asokamani, and A. K. Gogia, "Ti Based Biomaterials, the Ultimate Choice for Orthopaedic Implants – a Review," *Prog. Mater. Sci.,* **54** [3] 397-425 (2009).

8. C. G. Fawsitt, H. H. Z. Thom, L. P. Hunt, S. Nemes, A. W. Blom, N. J. Welton, W. Hollingworth, J. A. López-López, A. D. Beswick, A. Burston, O. Rolfson, G. Garellick, and E. M. R. Marques, "Choice of Prosthetic Implant Combinations in Total Hip Replacement: Cost-Effectiveness Analysis Using UK and Swedish Hip Joint Registries Data," *Value Health,* **22** [3] 303-12 (2019).

9. M. Mack, "Inflammation and Fibrosis," *Matrix Biol.,* **68-69,** 106-21 (2018).

10. P. Hajdu, R. Rácz, S. Biri, T. Radics, A. Csík, V. Takáts, C. Hegedűs, and S. Kökényesi, "Implantation of Multiply Charged Silicon Ions into Bioinert Zirconia," *Vacuum,* **164,** 15-7 (2019).

11. L. L Hench, "The Story of Bioglass®," *J. Mater. Sci.: Mater. Med.,* **17** [11] 967-78 (2006).

12. H. Y. Ang, H. Bulluck, P. Wong, S. S. Venkatraman, Y. Huang, and N. Foin, "Bioresorbable Stents: Current and Upcoming Bioresorbable Technologies," *Int. J. Cardiol.,* **228,** 931-9 (2017).

13. N. Gupta, D. Santhiya, S. Murugavel, A. Kumar, A. Aditya, M. Ganguli, and S. Gupta, "Effects of Transition Metal Ion Dopants (Ag, Cu and Fe) on the Structural, Mechanical and Antibacterial Properties of Bioactive Glass," *Colloids Surf., A,* **538,** 393-403 (2018).

14. D. Bellucci and V. Cannillo, "A Novel Bioactive Glass Containing Strontium and Magnesium with Ultra-High Crystallization Temperature," *Mater. Lett.,* **213,** 67-70 (2018).

15. O. Rodriguez, D. J. Curran, M. Papini, L. M. Placek, A. W. Wren, E. H. Schemitsch, P. Zalzal, and M. R. Towler, "Characterization of Silica-Based and Borate-Based, Titanium-Containing Bioactive Glasses for Coating Metallic Implants," *J. Non-Cryst. Solids,* **433,** 95-102 (2016).

16. P. Valerio, M. M. Pereira, A. M. Goes, and M. F. Leite, "The Effect of Ionic Products from Bioactive Glass Dissolution on Osteoblast Proliferation and Collagen Production," *Biomaterials,* **25** [15] 2941-8 (2004).

17. D. W. MacDonald, A. F. Chen, G.-C. Lee, G. R. Klein, M. A. Mont, S. M. Kurtz, H. E. Cates, M. J. Kraay, and C. M. Rimnac, "Fretting and Corrosion Damage in Taper Adapter Sleeves for Ceramic Heads: A Retrieval Study," *J. Arthroplasty,* **32** [9] 2887-91 (2017).

18. O. Borrero-Lopez, F. Guiberteau, Y. Zhang, and B. R. Lawn, "Wear of Ceramic-Based Dental Materials," *J. Mech. Behav. Biomed. Mater.,* **92,** 144-51 (2019).

19. E. Camposilvan, F. G. Marro, A. Mestra, and M. Anglada, "Enhanced Reliability of Yttria-Stabilized Zirconia for Dental Applications," *Acta Biomater.,* **17,** 36-46 (2015).

20. S. V.Dorozhkin, "Calcium Orthophosphate Bioceramics," *Ceram. Int.,* **41** [10] 13913-66 (2015).

21. L. Yu, Y. Li, K. Zhao, Y. Tang, Z. Cheng, J. Chen, Y. Zang, J. Wu, L. Kong, S. Liu, W. Lei, and Z. Wu, "A Novel Injectable Calcium Phosphate Cement-Bioactive Glass Composite for Bone Regeneration," *PLOS ONE,* **8** [4] e62570 (2013).

22. M. N. Rahaman, D. E. Day, B. Sonny Bal, Q. Fu, S. B. Jung, L. F. Bonewald, and A. P. Tomsia, "Bioactive Glass in Tissue Engineering," *Acta Biomater.,* **7** [6] 2355-73 (2011).

23. P.-F. Yang, X.-T. Nie, D.-D. Zhao, Z. Wang, L. Ren, H.-Y. Xu, J. Rittweger, and P. Shang, "Deformation Regimes of Collagen Fibrils in Cortical Bone Revealed by in Situ Morphology and Elastic Modulus Observations under Mechanical Loading," *J. Mech. Behav. Biomed. Mater.,* **79,** 115-21 (2018).

24. A. Mescher, *Junqueira's Basic Histology: Text and Atlas,* 13th ed. McGraw-Hill Education, 2013.

25. J. R. Woodard, A. J. Hilldore, S. K. Lan, C.J. Park, A. W. Morgan, J. A. C. Eurell, S. G. Clark, M. B. Wheeler, R. D. Jamison, and A. J. W. Johnson, "The Mechanical Properties and Osteoconductivity of Hydroxyapatite Bone Scaffolds with Multi-Scale Porosity," *Biomaterials,* **28** [1] 45-54 (2007).

26. P. K. Zysset, X. E. Guo, C. E. Hoffler, K. E. Moore, and S. A. Goldstein, "Elastic Modulus and Hardness of Cortical and Trabecular Bone Lamellae Measured by Nanoindentation in the Human Femur," *J. Biomech.,* **32** [10] 1005-12 (1999).

27. H. Aoki, *Science and Medical Applications of Hydroxyapatite*. Japanese Association of Apatite Science, [Tokyo], 1991.

28. D. Miura, T. Miyasaka, H. Aoki, Y. Aoyagi, and Y. Ishida, "Correlations among Bending Test Methods for Dental Hard Resins," *Dent. Mater. J.,* **36** [4] 491-6 (2017).

29. M. J. Mirzaali, J. J. Schwiedrzik, S. Thaiwichai, J. P. Best, J. Michler, P. K. Zysset, and U. Wolfram, "Mechanical Properties of Cortical Bone and Their Relationships with Age, Gender, Composition and Microindentation Properties in the Elderly," *Bone,* **93,** 196-211 (2016).

30. F. Libonati and L. Vergani, "Understanding the Structure–Property Relationship in Cortical Bone to Design a Biomimetic Composite," *Compos. Struct.,* **139,** 188-98 (2016).

31. A. J. Wagoner Johnson and B. A. Herschler, "A Review of the Mechanical Behavior of CaP and CaP/Polymer Composites for Applications in Bone Replacement and Repair," *Acta Biomater.,* **7** [1] 16-30 (2011).

32. J. Akbardoost, R. Amirafshari, O. Mohsenzade, and F. Berto, "Scaling Effect on the Fracture Toughness of Bone Materials Using MMTS Criterion," *J. Mech. Behav. Biomed. Mater.,* **85,** 72-9 (2018).

33. A. Feldmann, P. Ganser, L. Nolte, and P. Zysset, "Orthogonal Cutting of Cortical Bone: Temperature Elevation and Fracture Toughness," *Int. J. Machine Tools and Manuf.,* **118-119,** 1-11 (2017).

34. A. Carpinteri, F. Berto, G. Fortese, C. Ronchei, D. Scorza, and S. Vantadori, "Modified Two-Parameter Fracture Model for Bone," *Eng. Fract. Mech.,* **174,** 44-53 (2017).

35. J.-F. Stoltz, J. Magdalou, D. George, Y. Chen, Y. Li, N. De Isla, X. He, and Y. Remond, "Influence of Mechanical Forces on Bone: Introduction to Mechanobiology and Mechanical Adaptation Concept," *J. Cell. Immunother.,* **4** [1] 10-2 (2018).

36. C. H. Turner, A. Chandran, and R. M. V. Pidaparti, "The Anisotropy of Osteonal Bone and Its Ultrastructural Implications," *Bone,* **17** [1] 85-9 (1995).

37. J. Black, *Biological Performance of Materials: Fundamentals of Biocompatibility,* 3rd ed. CRC Press, Boca Raton, FL, 1999.

38. M. R. Forwood and C. H. Turner, "Skeletal Adaptations to Mechanical Usage: Results from Tibial Loading Studies in Rats," *Bone,* **17** [4, Supplement] S197-S205 (1995).

39. A. G. Robling, K. M. Duijvelaar, J. V. Geevers, N. Ohashi, and C. H. Turner, "Modulation of Appositional and Longitudinal Bone Growth in the Rat Ulna by Applied Static and Dynamic Force," *Bone,* **29** [2] 105-13 (2001).

40. M. Y. W. Suchanek, "Processing and Properties of Hydroxyapatite-Based Biomaterials for Use as Hard Tissue Replacement Implants," *J. Mater. Res.,* **13** [1] 94 - 117 (1997).

41. T. Kokubo, H. M. Kim, and M. Kawashita, "Novel Bioactive Materials with Different Mechanical Properties," *Biomaterials,* **24** [13] 2161-75 (2003).

42. J.-H. Chen, C. Liu, L. You, and C. A. Simmons, "Boning up on Wolff's Law: Mechanical Regulation of the Cells That Make and Maintain Bone," *J. Biomech.,* **43** [1] 108-18 (2010).

43. W. Wang and K. W. K. Yeung, "Bone Grafts and Biomaterials Substitutes for Bone Defect Repair: A review," *Bioact. Mater.,* **2** [4] 224-47 (2017).

44. N. Kohli, S. Ho, S. J. Brown, P. Sawadkar, V. Sharma, M. Snow, and E. García-Gareta, "Bone Remodelling in Vitro: Where Are We Headed?," *Bone,* **110,** 38-46 (2018).

45. S. L. Teitelbaum, "Bone Resorption by Osteoclasts," *Science,* **289** [5484] 1504-8 (2000).

46. R. F. Heary, N. Parvathreddy, S. Sampath, and N. Agarwal, "Elastic Modulus in the Selection of Interbody Implants," *J. Spine Surg. (Hong Kong),* **3** [2] 163-7 (2017).

47. J.-P. Bonjour, W. Kohrt, R. Levasseur, M. Warren, S. Whiting, and M. Kraenzlin, "Biochemical Markers for Assessment of Calcium Economy and Bone

Metabolism: Application in Clinical Trials from Pharmaceutical Agents to Nutritional Products," *Nutr. Res. Rev.*, **27** [2] 252-67 (2014).

48. G. Mabilleau, F. Pascaretti-Grizon, M. F. Baslé, and D. Chappard, "Depth and Volume of Resorption Induced by Osteoclasts Generated in the Presence of Rankl, TNF-Alpha/Il-1 or Light," *Cytokine,* **57** [2] 294-9 (2012).

49. P. J. Marie, "Strontium as Therapy for Osteoporosis," *Curr. Opin. Pharmacol.,* **5** [6] 633-6 (2005).

50. H. Autefage, F. Allen, H. M. Tang, C. Kallepitis, E. Gentleman, N. Reznikov, K. Nitiputri, A. Nommeots-Nomm, M. D. O'Donnell, C. Lange, B. M. Seidt, T. B. Kim, A. K. Solanki, F. Tallia, G. Young, P. D. Lee, B. F. Pierce, W. Wagermaier, P. Fratzl, A. Goodship, J. R. Jones, G. Blunn, and M. M. Stevens, "Multiscale Analyses Reveal Native-Like Lamellar Bone Repair and near Perfect Bone-Contact with Porous Strontium-Loaded Bioactive Glass," *Biomaterials,* **209,** 152-62 (2019).

51. Z. Y. Li, W. M. Lam, C. Yang, B. Xu, G. X. Ni, S. A. Abbah, K. M. C. Cheung, K. D. K. Luk, and W. W. Lu, "Chemical Composition, Crystal Size and Lattice Structural Changes after Incorporation of Strontium into Biomimetic Apatite," *Biomaterials,* **28** [7] 1452-60 (2007).

52. M. Arora and E. Arora, "The Promise of Silicon: Bone Regeneration and Increased Bone Density," *J. Arthroscopy Jt. Surg.,* **4** [3] 103-5 (2017).

53. J. R. Jones, "Review of Bioactive Glass: From Hench to Hybrids," *Acta Biomater.,* **9** [1] 4457-86 (2013).

54. K. Schwarz and D. B. Milne, "Growth-Promoting Effects of Silicon in Rats," *Nature,* **239** [5371] 333-4 (1972).

55. E. O'Neill, G. Awale, L. Daneshmandi, O. Umerah, and K. W. H. Lo, "The Roles of Ions on Bone Regeneration," *Drug Discov. Today,* **23** [4] 879-90 (2018).

56. R. L. Usala and J. G. Verbalis, "Disorders of Water and Sodium Homeostasis and Bone," *Curr. Opin. Endocr. Metab. Res.,* **3,** 83-92 (2018).

57. G. Madelin, A. Jerschow, and R. R. Regatte, "Sodium Relaxation Times in the Knee Joint in Vivo at 7T," *NMR Biomed.,* **25** [4] 530-7 (2012).

58. N. J. Lakhkar, I.-H. Lee, H.-W. Kim, V. Salih, I. B. Wall, and J. C. Knowles, "Bone Formation Controlled by Biologically Relevant Inorganic Ions: Role and Controlled Delivery from Phosphate-Based Glasses," *Adv. Drug Delivery Rev.,* **65** [4] 405-20 (2013).

59. C. Wang, G. Zhang, Z. Li, X. Zeng, Y. Xu, S. Zhao, H. Hu, Y. Zhang, and T. Ren, "Tribological Behavior of Ti-6Al-4V against Cortical Bone in Different Biolubricants," *J. Mech. Behav. Biomed. Mater.,* **90,** 460-71 (2019).

60. B. Wu, S. Xiong, Y. Guo, Y. Chen, P. Huang, and B. Yang, "Tooth-Colored Bioactive Titanium Alloy Prepared with Anodic Oxidation Method for Dental Implant Application," *Mater. Lett.*, **248,** 134-7 (2019).

61. A. Osaka, K. Tsuru, and S. Hayakawa, "Titania Derived from Combined Chemical and Thermal Treatments of Titanium: In Vitro Apatite Forming Ability," *Phosphorus Res. Bull.*, **17,** 130-41 (2004).

62. B. D. Boyan, T. W. Hummert, D. D. Dean, and Z. Schwartz, "Role of Material Surfaces in Regulating Bone and Cartilage Cell Response," *Biomaterials,* **17** [2] 137-46 (1996).

63. R. Samudrala, P. Abdul Azeem, V. Penugurti, and B. Manavathi, "Cytocompatibility Studies of Titania-Doped Calcium Borosilicate Bioactive Glasses in-Vitro," *Mater. Sci. Eng.: C,* **77,** 772-9 (2017).

64. V. Rajendran, A. V. Gayathri Devi, M. Azooz, and F. H. El-Batal, "Physicochemical Studies of Phosphate Based P2O5–Na2O–CaO–TiO2 Glasses for Biomedical Applications," *J. Non-Cryst. Solids,* **353** [1] 77-84 (2007).

65. A. V. Gayathri Devi, V. Rajendran, and N. Rajendran, "Structure, Solubility and Bioactivity in TiO2-Doped Phosphate-Based Bioglasses and Glass–Ceramics," *Mater. Chem. Phys.*, **124** [1] 312-8 (2010).

66. L. M. Placek, T. J. Keenan, Y. Li, C. Yatongchai, D. Pradhan, D. Boyd, N. P. Mellott, and A. W. Wren, "Investigating the Effect of TiO2 on the Structure and Biocompatibility of Bioactive Glass," *J. Biomed. Mater. Res., Part B,* **104** [8] 1703-12 (2016).

67. A. W. Wren, F. R. Laffir, A. Kidari, and M. R. Towler, "The Structural Role of Titanium in Ca–Sr–Zn–Si/Ti Glasses for Medical Applications," *J. Non-Cryst. Solids,* **357** [3] 1021-6 (2011).

68. M. Riaz, R. Zia, F. Saleemi, T. Hussain, F. Bashir, and H. Ikhram, "Effect of Ti+4 on in Vitro Bioactivity and Antibacterial Activity of Silicate Glass-Ceramics," *Mater. Sci. Eng.: C,* **69,** 1058-67 (2016).

69. B. Fartash, H. Liao, J. Li, N. Fouda, and L. Hermansson, "Long-Term Evaluation of Titania-Based Ceramics Compared with Commercially Pure Titanium in Vivo," *J. Mater. Sci.: Mater. Med.,* **6** [8] 451-4 (1995).

70. W. C. A. Vrouwenvelder, C. G. Groot, and K. de Groot, "Better Histology and Biochemistry for Osteoblasts Cultured on Titanium-Doped Bioactive Glass: Bioglass 45s5 Compared with Iron-, Titanium-, Fluorine- and Boron-Containing Bioactive Glasses," *Biomaterials,* **15** [2] 97-106 (1994).

71. J. A. Williams, R. W. Billington, and G. J. Pearson, "The Effect of the Disc Support System on Biaxial Tensile Strength of a Glass Ionomer Cement," *Dent. Mater.,* **18** [5] 376-9 (2002).

72. B.-J. Choi, S. Yoon, Y.-W. Im, J.-H. Lee, H.-J. Jung, and H.-H. Lee, "Uniaxial/Biaxial Flexure Strengths and Elastic Properties of Resin-Composite Block Materials for Cad/Cam," *Dent. Mater.,* **35** [2] 389-401 (2019).

73. S. S. Chon, L. Piraino, S. Mokhtari, E. A. Krull, A. Coughlan, Y. Gong, N. P. Mellott, T. J. Keenan, and A. W. Wren, "Synthesis, Characterization and Solubility Analysis of Amorphous Sio2-CaO-Na2O-P2O5 Scaffolds for Hard Tissue Repair," *J. Non-Cryst. Solids,* **490** 1-12 (2018).

74. S. Pourshahrestani, E. Zeimaran, N. Adib Kadri, N. Gargiulo, S. Samuel, S. Naveen, T. Zaman, and M. Towler, "Gallium-Containing Mesoporous Bioactive Glass with Potent Hemostatic Activity and Antibacterial Efficacy," *J. Mater. Chem. B,* **4** 71 (2016).

75. G. Țăran, K. Magyari, A. Topan, A. Vulpoi, and L. Baia, "Improved Bioactivity Properties of Sio2-CaO-P2O5 Glasses by Using Calcium L-Lactate Pentahydrate as Calcium Oxide Precursor," *J. Non-Cryst. Solids,* **498** 199-203 (2018).

76. A. Li, H. Ren, Y. Cui, C. Wang, X. Zhou, H. Lin, and D. Qiu, "Detailed Structure of a New Bioactive Glass Composition for the Design of Bone Repair Materials," *J. Non-Crys. Solids,* **475** 10-4 (2017).

77. J. Serra, P. González, S. Liste, S. Chiussi, B. León, M. Pérez-Amor, H. O. Ylänen, and M. Hupa, "Influence of the Non-Bridging Oxygen Groups on the Bioactivity of Silicate Glasses," *J. Mater. Sci.: Mater. Med.,* **13** [12] 1221-5 (2002).

78. A. Mirza, M. Riaz, R. Zia, T. Hussain, and F. Bashir, "Effect of Temperature on Mechanical and Bioactive Properties of Glass-Ceramics," *J. Alloys Compd.,* **726** 348-51 (2017).

79. M. Plewinski, K. Schickle, M. Lindner, A. Kirsten, M. Weber, and H. Fischer, "The Effect of Crystallization of Bioactive Bioglass 45s5 on Apatite Formation and Degradation," *Dent. Mater.,* **29** [12] 1256-64 (2013).

80. N. Lotfibakhshaiesh, D. S. Brauer, and R. G. Hill, "Bioactive Glass Engineered Coatings for Ti6Al4V Alloys: Influence of Strontium Substitution for Calcium on Sintering Behaviour," *J. Non-Cryst. Solids,* **356** [44] 2583-90 (2010).

81. Y. Pan, Y. Chen, and Q. Shen, "Flexural Mechanical Properties of Functional Gradient Hydroxyapatite Reinforced Polyetheretherketone Biocomposites," *J. Mater. Sci. Technol.*, **32** [1] 34-40 (2016).

82. Y. Li, A. Coughlan, F. R. Laffir, D. Pradhan, N. P. Mellott, and A. W. Wren, "Investigating the Mechanical Durability of Bioactive Glasses as a Function of Structure, Solubility and Incubation Time," *J. Non-Cryst. Solids,* **380** 25-34 (2013).

83. Z. Kang, B. Yu, S. Fu, D. Li, X. Zhang, Z. Qian, Z. Zhong, B. Yu, H. Ding, Y. Zhu, and J. Huang, "Three-Dimensional Printing of Catio3 Incorporated Porous B-Ca2sio4 Composite Scaffolds for Bone Regeneration," *Applied Materials Today,* **16** 132-40 (2019).

84. N. S. G. Alexander Hoppe, Aldo R. Boccaccini, "A Review of the Biological Response to Ionic Dissolution Products from Bioactive Glasses and Glass-Ceramics," *Biomaterials,* **32** 2757-74 (2011).